ELSEVIER

Journal of Neuroscience Methods 154 (2006) 116–133

JOURNAL OF NEUROSCIENCE METHODS

www.elsevier.com/locate/jneumeth

Current-source density estimation based on inversion of electrostatic forward solution: Effects of finite extent of neuronal activity and conductivity discontinuities

Klas H. Pettersen [a], Anna Devor [b,c], Istvan Ulbert [b,d], Anders M. Dale [c], Gaute T. Einevoll [a,*]

[a] *Department of Mathematical Sciences and Technology, Norwegian University of Life Sciences, P.O. Box 5003, N-1432 Ås, Norway*
[b] *Athinoula A. Martinos Center, Massachusetts General Hospital, 149 13th Street, Charlestown, MA 02129, USA*
[c] *Departments of Radiology and Neurosciences, University of California, San Diego, 9500 Gilman Drive, La Jolla, CA 92093-0662, USA*
[d] *Institute for Psychology of the Hungarian Academy of Sciences, Budapest, Hungary*

Received 5 October 2005; received in revised form 19 November 2005; accepted 5 December 2005

Abstract

A new method for estimation of current-source density (CSD) from local field potentials is presented. This *inverse CSD (iCSD)* method is based on explicit inversion of the electrostatic forward solution and can be applied to data from multielectrode arrays with various geometries. Here, the method is applied to linear-array (laminar) electrode data. Three iCSD methods are considered: the CSD is assumed to have cylindrical symmetry and be (i) localized in infinitely thin discs, (ii) step-wise constant or (iii) continuous and smoothly varying (using cubic splines) in the vertical direction. For spatially confined CSD distributions the standard CSD method, involving a discrete double derivative, is seen in model calculations to give significant estimation errors when the lateral source dimension is comparable to the size of a cortical column (less than ∼1 mm). Further, discontinuities in the extracellular conductivity are seen to potentially give sizable errors for even wider source distributions. The iCSD methods are seen to give excellent estimates when the correct lateral source dimension and spatial distribution of conductivity are incorporated. To illustrate the application to real data, iCSD estimates of stimulus-evoked responses measured with laminar electrodes in the rat somatosensory (barrel) cortex are compared to estimates from the standard CSD method.

Keywords: Local field potentials; Current-source density; CSD; Multielectrode; Laminar electrode; Barrel cortex

1. Introduction

The technology for large-scale electrical recording of neural activity is rapidly improving, and this offers better opportunities for going beyond standard single-unit studies and measure the activity from populations of neurons (Nadasdy et al., 1998; Buzsaki, 2004). Various types of multisite electrodes are used to simultaneously record firing of action potentials from numerous neurons, but new methods for data analysis are needed to fully exploit recordings of local field potentials from, for example, multishank laminar electrodes (Buzsaki, 2004).

Local field potentials, i.e., the low-frequency part of extracellularly recorded potentials, are thought to predominantly stem from dendritic processing of synaptic inputs, but a direct interpretation in terms of the underlying neural activity is difficult (Freeman and Nicholson, 1975). A standard measurement procedure has been to record the field potential at equidistant, linearly positioned electrode contacts using a laminar electrode vertically penetrating the cortical layers (see, e.g., Rappelsberger et al. (1981), Mitzdorf (1985), Nadasdy et al. (1998), Ulbert et al. (2001)). Under the assumptions of homogeneous cortical in-plane activity, constant extracellular electrical conductivity and equidistant electrode contacts, the *current-source density (CSD)* can be estimated from a double spatial derivative of the recorded potentials (Freeman and Nicholson, 1975; Rappelsberger et al., 1981; Nakagawa and Matsumoto, 2000). This standard CSD estimation method only predicts the CSD at the interior electrode positions. Vaknin et al. (1988) suggested a procedure for also obtaining CSD estimates at the first and last electrode based on the assumption that the potential varies negligibly above the first and below the last electrode.

Cortical activity has a characteristic columnar organization (Hubel and Wiesel, 1977; Mountcastle, 1997), and the in-plane homogeneity assumption is questionable. For the rat barrel

* Corresponding author. +47 64965433; fax: +47 64965401.
E-mail address: Gaute.Einevoll@umb.no (G.T. Einevoll).

0165-0270/$ – see front matter © 2006 Elsevier B.V. All rights reserved.
doi:10.1016/j.jneumeth.2005.12.005

cortex, where each whisker has a dedicated barrel column, Di and Barth (1991) found the surface potential measured above the barrels to be varying on the submillimeter scale following stimulation of the principal whisker. Nicholson and co-workers (Nicholson and Llinas, 1971; Nicholson and Freeman, 1975; Freeman and Nicholson, 1975) studied cerebellar activity in various species and estimated the effective size of the columnar activity to be so small (∼0.5 mm; Nicholson and Llinas, 1971) that the applicability of standard CSD analysis was questioned. Indeed they recommended and later pursued a full three-dimensional CSD analysis where the potential was measured in all spatial directions (Nicholson and Llinas, 1975). The spatial extension of neural activity will in general depend on, for example, the type of cortex, type of stimulus (if stimulus-evoked responses are considered) and level and type of anesthesia.

In the present paper we develop a general method for estimation of CSDs from measured local field potentials where situations such as (i) spatially confined cortical activity and (ii) spatially varying extracellular conductivity can be handled. The method, labeled the *inverse CSD (iCSD) method*, is based on the explicit inversion of the electrostatic forward solution. The calculation of the electrical potential from a given CSD distribution is in principle straightforward, and in our method this is exploited to solve the inverse problem, i.e., estimate the CSD distribution parameterized by N parameters from N measurements of the potential.

Preliminary results from this project have been presented earlier in poster format (Pettersen et al., 2004).

2. Methods

2.1. Matrix formulation of standard CSD method

A common starting point for the estimation of the current-source density $C(x, y, x)$ from the extracellular field potential $\phi(x, y, z)$ is (Nicholson and Freeman, 1975; Mitzdorf, 1985)

$$\nabla \cdot (\sigma \nabla \phi) = -C, \tag{1}$$

where σ represents the electrical conductivity tensor which in general depends on position. The derivation of this relationship is based on the quasistatic approximation, and this approximation appears to be valid for the low temporal frequencies characteristic for the field potentials of interest (Mitzdorf, 1985; Hämäläinen et al., 1993). It also assumes the extracellular medium to act as a volume conductor and to be ohmic in the relevant frequency range.

The conductivity tensor is symmetric, and by a suitable choice of coordinate system it can be made diagonal (Nicholson and Freeman, 1975). In cortical applications of CSD analysis, the z-axis is usually defined to be perpendicular to the cortical layers while the x- and y-axes span out the in-layer plane. For the case of homogeneous and isotropic conductivity ($\sigma_x = \sigma_y = \sigma_z = \sigma$), Eq. (1) further simplifies to

$$\sigma \left(\frac{\partial^2 \phi}{\partial x^2} + \frac{\partial^2 \phi}{\partial y^2} + \frac{\partial^2 \phi}{\partial z^2} \right) = -C(x, y, z). \tag{2}$$

In most applications of the CSD method, the potential ϕ is assumed to be constant in the in-plane directions, so that the CSD simply is given by the double spatial derivative in z-direction,

$$\sigma \frac{\partial^2 \phi}{\partial z^2} = -C(z). \tag{3}$$

This approximation corresponds to assuming that the neuronal current sources effectively are infinitely large planes with no variation in the neural activity in the in-plane directions.

With laminar electrodes one only measures the potential ϕ for a discrete set of cortical depths with a fixed spacing h. The simplest formula for approximating the double spatial derivative in Eq. (3) from this set of discrete data points follows from the definition of the derivative. In Freeman and Nicholson (1975), this estimator is denoted D_1,

$$D_1(z) = \frac{\phi(z + h) - 2\phi(z) + \phi(z - h)}{h^2}. \tag{4}$$

With measurements of the potential ϕ at N equidistant electrode contact positions, the CSD at the $N - 2$ interior electrode positions can be directly estimated using this formula. However, the CSD at the first and last electrode positions cannot be estimated using such a three-point formula.

In the *inverse CSD* method outlined below, a matrix representation is used to formulate the estimation problem. Here, the N measurements of the potential ϕ are represented by an N-dimensional column vector $\mathbf{\Phi}$. For the standard CSD method where $N - 2$ values of the CSD are estimated, the estimated CSD values $\hat{C}$ are likewise represented by the $N - 2$-dimensional column vector $\hat{\mathbf{C}}$. From Eqs. (3) and (4) it thus follows that the standard CSD method can be represented in matrix form as

$$\hat{\mathbf{C}} = -\sigma \mathbf{D}_1 \mathbf{\Phi}, \tag{5}$$

where $\hat{\mathbf{C}} = [\hat{C}_2\ \hat{C}_3\ \dots\ \hat{C}_{N-1}]^{\mathrm{T}}$, $\mathbf{\Phi} = [\phi_1\ \phi_2\ \dots\ \phi_N]^{\mathrm{T}}$, and

$$\mathbf{D}_1 = \frac{1}{h^2} \begin{bmatrix} 1 & -2 & 1 & 0 & 0 & 0 & \dots & & \dots & 0 \\ 0 & 1 & -2 & 1 & 0 & 0 & \dots & & \dots & 0 \\ . & . & . & . & . & . & \dots & & \dots & . \\ 0 & 0 & \dots & & & & \dots & 0 & 1 & -2 & 1 \end{bmatrix}. \tag{6}$$

Here, $\mathbf{D}_1$ is a $(N - 2) \times N$ matrix, and ϕ_i and $\hat{C}_i$ represent the potential and estimated CSD, respectively, at electrode position z_i.

2.2. Inverse CSD method

In the matrix formulation of the standard CSD method in Eq. (5) the matrix $\mathbf{D}_1$ estimates the CSD based on field potential data contained in $\mathbf{\Phi}$. The opposite problem of calculating field potentials when the CSD is given, can be found directly by solving the electrostatic forward problem. The field potential $\phi(x, y, z)$ produced by a point current-source I_{C} at the origin of an infinite volume conductor having constant and isotropic electrical

conductivity σ, is given by (Nicholson and Freeman, 1975)

$$\phi(x, y, z) = \frac{I_C}{4\pi\sigma\sqrt{x^2 + y^2 + z^2}}. \quad (7)$$

This forward solution can be used to calculate the field potential ϕ for any distribution of current point sources since the contributions add up linearly.

In analogy to Eq. (5) a matrix formulation of this forward solution is given by $\mathbf{\Phi} = \mathbf{FC}$. The basic idea of the inverse CSD method is to use standard electrostatic theory to calculate the matrix $\mathbf{F}$, and then use the inverse of this matrix $\mathbf{F}^{-1}$ to estimate the CSD via $\hat{\mathbf{C}} = \mathbf{F}^{-1}\mathbf{\Phi}$. With N separate measurements of the field potential ϕ, one can only estimate N parameters describing the CSD. One thus has to make additional assumptions about how these parameters determine the spatial CSD distribution. The standard CSD method assumes the current sources evenly distributed in infinite planes. In the derivation of the inverse CSD methods below we instead consider the more general case where the current sources are evenly distributed within cylindrical discs of radius R. The method thus assumes a situation where the CSD is restricted to a cylindrical column, and the infinite plane situation is obtained in the limit $R \to \infty$.

We here consider three iCSD methods for constructing the matrix $\mathbf{F}$: the *δ-source* iCSD method assumes infinitely thin current-source discs, the *step* iCSD method assumes step-wise constant CSD between the electrode contacts, while the *spline* iCSD method assumes a smoothly varying CSD. The methods each have their own merits and disadvantages: while the spline iCSD method assumes a more realistic CSD distribution, the δ-source and step iCSD methods are easier to implement and generalize to more complex source geometries.

2.2.1. δ-Source iCSD method

We first consider an infinitely thin circular disc of radius R with constant planar current-source density (current-source per area) C_p. Mathematically this corresponds to a δ-function in the z-direction, and we thus label this version of the method for the *δ-source iCSD* method. The current disc lies in the xy-plane with its center at $x = y = 0$. The potential $\phi(z)$ at the center axis of such a current disc positioned at the height z' is given by (Nicholson and Llinas, 1971)

$$\phi(z, z') = \frac{C_p}{2\sigma}(\sqrt{(z - z')^2 + R^2} - |z - z'|). \quad (8)$$

It is convenient in the following to replace the planar source density (C_p) with the equivalent (volume) current-source density $C = C_p/h$. This corresponds to the current-source density one would obtain if the planar current instead was evenly distributed in a box of height h in which the disc is embedded.

If we assume the measured field potentials to be due to a sum of contributions from such discs positioned at the N electrode contact points, the potential at electrode position z_j will be

$$\phi(z_j) = \sum_{i=1}^{N} \left[\frac{h}{2\sigma} \left(\sqrt{(z_j - z_i)^2 + R^2} - |z_j - z_i| \right) \right] C(z_i)$$
$$= \sum_{i=1}^{N} F_{ji}\, C(z_i), \quad (9)$$

where we have introduced

$$F_{ji} = \frac{h}{2\sigma} \left(\sqrt{(z_j - z_i)^2 + R^2} - |z_j - z_i| \right)$$
$$= \frac{h^2}{2\sigma} \left(\sqrt{(j - i)^2 + (R/h)^2} - |j - i| \right). \quad (10)$$

In the final step we have assumed that the electrode positions z_j are given by $z_j = z_1 + (j - 1)h$, where z_1 is the position of the first electrode contact point.

Eq. (9) represents a system of N equations with N unknown values $C_i = C(z_i)$ describing the CSD, and N measured potentials $\phi_j = \phi(z_j)$. It can be expressed in matrix form as $\mathbf{\Phi} = \mathbf{FC}$, where $\mathbf{\Phi} = [\phi_1\ \phi_2\ \ldots\ \phi_N]^T$, $\mathbf{C} = [C_1\ C_2\ \ldots\ C_N]^T$ and $\mathbf{F}$ is an $N \times N$-matrix with elements given by Eq. (10).

The solution of the forward problem is now represented by $\mathbf{\Phi}$, while $\mathbf{F}$ is the transformation matrix required to obtain the forward solution. The matrix $\mathbf{F}$ will in general be non-singular and will thus have an inverse matrix $\mathbf{F}^{-1}$. An estimator $\hat{\mathbf{C}}$ for the CSD based on potentials measured at the cylinder center axis ($\mathbf{\Phi}$) is thus given by $\hat{\mathbf{C}} = \mathbf{F}^{-1}\mathbf{\Phi}$. The matrix $\mathbf{F}$ (and thus $\mathbf{F}^{-1}$) will depend on the radius R of the source discs. This simply reflects that the potential measured at the center axis will not only depend on the depth profile of the CSD, but also the radial extension of the source.

The situation where the source radius R becomes very large so that the disc sources approach infinite planes, is of particular interest. In Appendix A, we show that when R becomes much larger than the spatial extension of the laminar electrode (Nh), the δ-source iCSD method (Eq. (10)) predicts the same CSD as the standard CSD method for the $N - 2$ interior electrode positions. We also find that when the current-source densities are balanced, i.e., $\sum_i C_i = 0$, the iCSD method agrees with the procedure suggested by Vaknin et al. (1988) for obtaining CSD estimates at the first and last electrode positions (but only in the $R \to \infty$ limit). However, when the current-source densities are unbalanced ($\sum_i C_i \neq 0$), the Vaknin-procedure is found to be incorrect.

The dependence of the weight coefficients in the matrix $\mathbf{F}^{-1}$ is illustrated in Fig. 1. For all population diameters the central weight, i.e., the weight contribution from the measured potentials to the estimated CSD at the same electrode position, is found to have the largest magnitude. For large population diameters the weight coefficients (for the interior contact positions) is seen to follow the characteristic '$(-1) : 2 : (-1)$'-pattern around the central position. For smaller diameters, however, the weight coefficients for the nearest neighbors are reduced, and all weight is eventually put on the central position (as discussed in Appendix A).

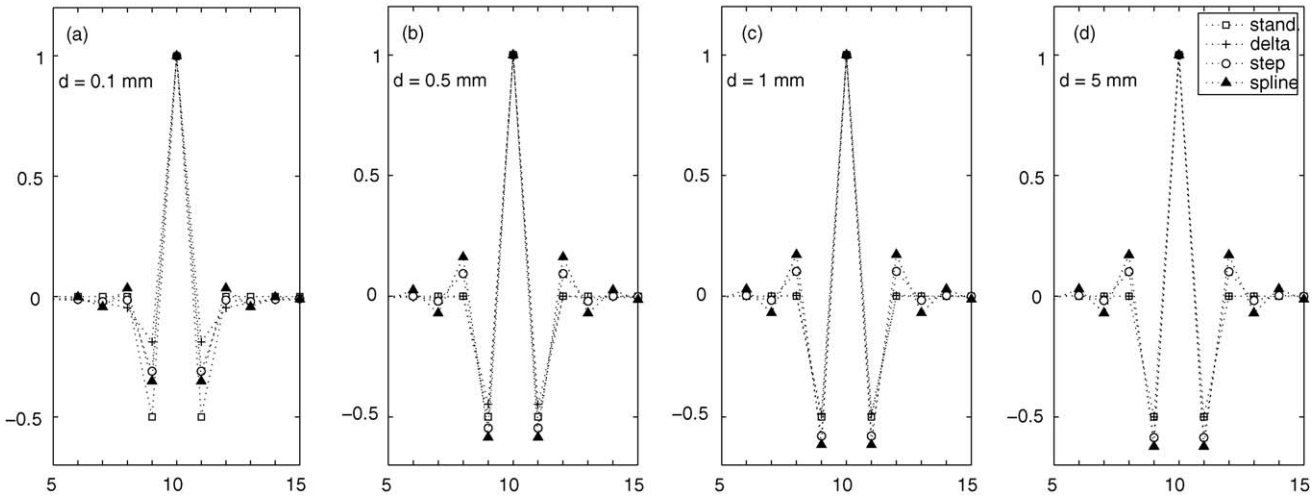

Fig. 1. Illustration of weight coefficients, i.e., matrix elements in the matrix $\mathbf{F}^{-1}$, for a set of different current-source diameters, d. (a) $d = 0.1$ mm, (b) $d = 0.5$ mm, (c) $d = 1$ mm and (d) $d = 5$ mm. Here, there are 20 electrode contacts with a spacing of 0.1 mm, and the matrix elements $(\mathbf{F}^{-1})_{ji}$ corresponding to the row for electrode contact no. 10 are shown. These matrix elements determine the sum estimating the CSD at electrode position no. 10 from the measured potentials. Results for the standard CSD method (squares, cf. Eq. (6)), δ-source iCSD (pluses, cf. Eq. (10)), step iCSD (circles, cf. Eq. (12)) and spline iCSD (triangles, cf. Eq. (28)) are shown. The displayed matrix elements are normalized to have unit magnitude at the central position. Dotted lines have been added to guide the eye.

2.2.2. Step iCSD method

In the above δ-source iCSD method we assumed all current sources to be localized in infinitely thin discs positioned at the electrode contact points. We now consider a modified method, labeled the *step iCSD* method, where the current-source is assumed to be step-wise constant in the z-direction. Thus, we assume that the δ-sources are extended to cylindrical boxes of height h symmetrically embedding the former infinitely thin discs positioned at the electrode positions.

In this case the potential measured at the center axis at position z_j due to a cylindrical current box with constant current-source density C_i around the electrode position z_i, is given by (cf. Eq. (8))

$$\phi(z_j) = C_i \int_{z_i-h/2}^{z_i+h/2} \frac{1}{2\sigma} \left(\sqrt{(z_j - z')^2 + R^2} - |z_j - z'| \right) \mathrm{d}z'. \tag{11}$$

Thus, the forward solution can be formulated in the matrix form $\mathbf{\Phi} = \mathbf{FC}$ where the matrix elements are given by

$$F_{ji} = \int_{z_i-h/2}^{z_i+h/2} \frac{1}{2\sigma} \left(\sqrt{(z_j - z')^2 + R^2} - |z_j - z'| \right) \mathrm{d}z'. \tag{12}$$

This integral can be evaluated exactly, but the resulting formula is not shown here.

Due to the finite spatial extension of the CSD sources in the vertical direction, the matrix $\mathbf{F}$ will be different from the corresponding matrix in the δ-source case (Eq. (10)). Likewise the inverse matrix $\mathbf{F}^{-1}$ will be different. This is illustrated in Fig. 1 where it is seen that the weight matrix in the infinite plane limit ($d = 5$ mm) differs from the '$(-1) : 2 : (-1)$'-pattern inherent in the standard CSD three-point formula (and δ-source iCSD method). There are non-negligible contributions from more distant neighbors; the box-like current sources alone results in an estimation formula involving more than three spatial points. Moreover, the weights of the nearest-neighbor electrode positions are larger in magnitude compared to the central position than predicted by the standard three-point formula. For smaller population diameters the weight of the central position grows and the weight distribution becomes narrower, in accordance with the observation for the δ-source situation described above.

2.2.3. Spline iCSD method

The assumption of a step-wise constant CSD between the electrode contact points is physiologically more realistic than the δ-source assumption inherent in the standard CSD method. An obvious extension is to assume the CSD between the contact points to be piecewise linear and to require continuity at the interface points. However, this would introduce discontinuities in the first derivatives. It is thus even more natural to assume a smoothly varying CSD between the electrode contacts. Here, we develop such an iCSD method, labeled the *spline iCSD* method, using cubic splines (Kreyzig, 1999). The smoothly varying CSD in the z-direction is constructed by interpolating a set of cubic polynomials requiring the CSD and the first and second derivatives in the z-direction to be continuous. As before we consider a homogeneous disc distribution in the in-plane (x, y) directions. The spline iCSD method is described in detail in Appendix B.

An example comparison of the weight matrices $(\mathbf{F}^{-1})_{ji}$ for the standard CSD, δ-source iCSD, step iCSD and spline iCSD methods are shown in Fig. 1. We see that the step iCSD and spline iCSD methods have non-negligible weights on the next-nearest neighbor electrode contacts (also in the large R limit). The spline iCSD method is even seen to have some weight on the third nearest neighbor which corresponds to including potentials from seven electrode positions in the estimate of the CSD at the central position.

2.3. Dependence on electrical conductivity

In the above we have assumed the extracellular conductivity to be both spatially constant and isotropic ($\sigma_x = \sigma_y = \sigma_z = \sigma$). However, the results generalize straightforwardly to the case where the vertical conductivity σ_z differs from the lateral conductivities ($\sigma_x = \sigma_y = \sigma_l$). Using an appropriately modified version of the expression for the field potential from a point current-source (Nicholson and Freeman, 1975), we find that the potential at the center axis over planar, circular current sources is still found to be given by Eq. (8) with a modified effective disc radius, $R \to \sqrt{\sigma_z/\sigma_l}\, R$, and $\sigma \to \sigma_z$.

The inverse CSD method can also be extended to incorporate effects of a different extracellular conductivity above the cortical surface. In experiments with laminar electrodes substances like saline (with a high conductivity) or oil (with a very low conductivity) are commonly added to prevent drying of the brain. This will affect the measured potential generated by the underlying cortical current-source density. The boundary conditions inferred on the electrostatic problem due to such a conductivity jump at the cortical surface can be included by using the method of images (Nicholson and Llinas, 1971). With the cortical surface defined to be at $z = 0$ with $\sigma = \sigma_0$ above cortex ($z < 0$), the expression for the potential $\phi(z, z')$ in Eq. (8) generalizes to

$$\phi'(z, z') = \phi(z, z') + \frac{\sigma - \sigma_0}{\sigma + \sigma_0}\phi(z, -z'). \tag{13}$$

Correspondingly, the modified matrix elements F_{ji} are obtained by a similar replacement in the formula in Eq. (10) for the δ-source iCSD method, and in the integrands in Eqs. (12) and (23) for the step iCSD and spline iCSD methods, respectively.

2.4. Noise filtering

Differences in gain between electrode contacts and deviations from the assumption of equidistant electrode contact positions will produce spatial noise. The discrete three-point formula in Eq. (4) will by itself filter out some high spatial-frequency noise (Freeman and Nicholson, 1975). In addition, a three-point Hamming filter is often used to further reduce such noise, resulting in a five-point formula for the estimation of the CSD from the measured potentials (Rappelsberger et al., 1981; Ulbert et al., 2001). This means that the CSD is only estimated at $N - 4$ interior positions, even though the edge-interpolation method suggested by Vaknin et al. (1988) can give CSD estimates at two more positions. Freeman and Nicholson (1975) argued that a variation of the three-point formula where the next-nearest neighbor electrode contact positions are used, could be the best compromise for reducing spatial noise while maintaining a satisfactory spatial resolution. Again, this method gives CSD estimates only at $N - 4$ interior positions.

In the inverse CSD method a three-point Hamming filter could be applied on the N potential recordings to reduce spatial noise prior to further analysis. This would, however, reduce the number of potentials used in the subsequent CSD estimate to $N - 2$, and the spatial range for which the CSD could be estimated would be reduced. In the inverse CSD methods it is more natural to spatially filter the resulting estimated CSDs instead of filtering the potentials beforehand. Both the step iCSD and the spline iCSD methods inherently assume a non-zero CSD between the electrodes, and a continuous filter can thus be used. (For the δ-source iCSD method such a continuous filter will effectively correspond to a discrete filter analogous to the Hamming filter.)

Here, we use a Gaussian spatial filter which is convolved with the estimated CSD from the unfiltered potentials to produce a spatially smoothed CSD estimate. By assuming the CSD to be zero outside the spatial range of the estimated CSD, a smoothed CSD estimate can be obtained for all spatial positions.

2.5. Off-center electrode placement

In the above we have considered the laminar electrode to be positioned at the center axis of a cylindrical current-source. The iCSD method can straightforwardly be generalized to, for example, the situation where the laminar electrode is positioned off-center (but still parallel to the center axis). However, in this case a three-dimensional integral must be evaluated numerically to obtain the forward solution. This is done by using the general formula (Nicholson and Llinas, 1971; Jackson, 1998)

$$\phi(x, y, z) = \frac{1}{4\pi\sigma}\int\int\int_{V'} \times \frac{C(x', y', z')}{\sqrt{(x - x')^2 + (y - y')^2 + (z - z')^2}}\,\mathrm{d}x'\mathrm{d}y'\mathrm{d}z' \tag{14}$$

where the volume integral covers the current sources.

For example, for the step iCSD method the matrix element F_{ji} in Eq. (12) is now given by

$$F_{ji} = \frac{1}{4\pi\sigma}\int_{z_i - h/2}^{z_i + h/2}\int\int_{r' < R} \times \frac{1}{\sqrt{(x_\mathrm{e} - x')^2 + (y_\mathrm{e} - y')^2 + (z_j - z')^2}}\,\mathrm{d}x'\mathrm{d}y'\mathrm{d}z', \tag{15}$$

where $r' = \sqrt{x'^2 + y'^2}$, R is the radius of the cylindrical source and $[x_\mathrm{e}, y_\mathrm{e}]$ denotes the lateral position of the laminar electrode axis. (Note that the singularity in the integrand can be dealt with in the numerical evaluation of the integral by use of so called a-potentials in a limiting procedure, see p. 35 in Jackson (1998).)

2.6. Experimental procedure

An example laminar electrode recording from rat somatosensory (barrel) cortex illustrates the application of the inverse CSD method to real data. The barrel cortex in rat is a well-studied example of topographic mapping where each of the large facial vibrissa (whiskers) is mapped onto a specific cortical area, called a barrel (Woolsey and Van der Loos, 1970). In our group the barrel cortex has been used to study hemodynamic and neuronal activity following a tactile whisker stimulation of a single

whisker (Devor et al., 2003, 2005). A representative example of neuronal activity recordings using a laminar electrode array is used to illustrate the present method.

Male Sprague–Dawley rats (250–350 g, Taconic) were used for the experiments. Glycopyrrolate (0.5 mg/kg, i.m.) was administered 10 min before the initiation of anesthesia. Rats were anesthetized with a single dose of ketamine hydrochloride (50 mg/kg, i.p.), supplemented with sodium pentobarbital (12 mg/kg) during the surgery. During the rest of the experiment animals were supplemented by constant i.p. infusion of 50 mg/kg/h of ketamine hydrochloride. During surgery a tracheotomy was performed, cannulas were inserted in the femoral artery and vein. All incisions were infiltrated with 2% lidocaine. Following tracheotomy, rats were mechanically ventilated with 30% O_2 in air. Ventilation parameters were adjusted to maintain Pa_{CO_2} between 35 and 45 mm Hg, Pa_{O_2} between 140 and 180 mm Hg, and pH between 7.35 and 7.45. Heart rate, ECG and blood pressure were monitored continuously. Body temperature was maintained at 37.0 °C ± 0.5 °C with a homeothermic blanket (Harvard Apparatus, Holliston, MA, USA). The animal was fixed in a stereotaxic frame. An area of skull overlying the primary somatosensory cortex was exposed and then thinned with a dental burr. The thinned skull was removed and the dura matter dissected to expose the cortical surface. A barrier of dental acrillic was built around the border of the exposure and filled with mineral oil. Mapping with a single metal microelectrode (FHC, 5–7 MΩ) was done to determine the positioning of the laminar electrode array. The optimal position was identified by listening to an audio monitor while stimulating different whiskers. Following the mapping procedure, the electrode was withdrawn, and the array was slowly introduced at the same location perpendicular to the cortical surface. Contact no. 1 was positioned at the cortical surface using visual control. A linear-array multielectrode with 23 contacts spaced at 0.1 mm (Ulbert et al., 2001) was used, and laminar signals were filtered between 0.1 and 500 Hz to produce the local field potentials.

Single whiskers were deflected upward by a wire loop coupled to a computer-controlled piezoelectric stimulator. We employed a fast, randomized event-related stimulus presentation paradigm. The stimulus sequence was optimized for event-related response estimation efficiency using the approach described by Dale (1999). The stimulation paradigm consisted of single deflections of varying amplitude with interstimulus interval (ISI) of 1 s. We used nine stimulus amplitudes. Intervening amplitudes were spaced with equal increments on a linear scale. The stimulus angular velocity increased from 203 deg/s (vertical displacement of 0.24 mm, amplitude 1) to 969 deg/s (vertical displacement of 1.2 mm, amplitude 9).

3. Results

3.1. Model-based test of iCSD method

We first performed a model study. Knowing the correct CSD allowed us to readily assess the accuracy of the methods; an option not available when using experimental data. In Fig. 2, the depth profile of the three model CSD distributions is shown. The first distribution consists of a region of constant positive current-source density (source) above a region of constant negative current-source density (sink). A similar highly idealized square-function distribution was also considered by Nicholson and Freeman (1975) to illustrate the limitations of the standard CSD method. Physiological CSD distributions are not expected to change so abruptly. In the second model distribution we thus assume a smoother, sinusoidally varying CSD distribution, and the third model distribution is a sum over two Gaussian functions (see caption of Fig. 2 for a precise definition of these distributions). All model CSD distributions are balanced, i.e., they sum to zero. The magnitudes of the CSD distributions have been chosen to give extracellular potentials with a magnitude of about 1 mV with our choice $\sigma = 0.3$ S/m for extracellular conductivity (Hämäläinen et al., 1993).

3.1.1. Potentials from model distributions

The electrical potential due to a cylindrical CSD distribution with depth profile given by these model distributions can now be calculated. When the electrical conductivity σ is constant, Eq. (14) can be used directly, while the expression must be modified according to the aforementioned method of images when there is a different conductivity above cortex.

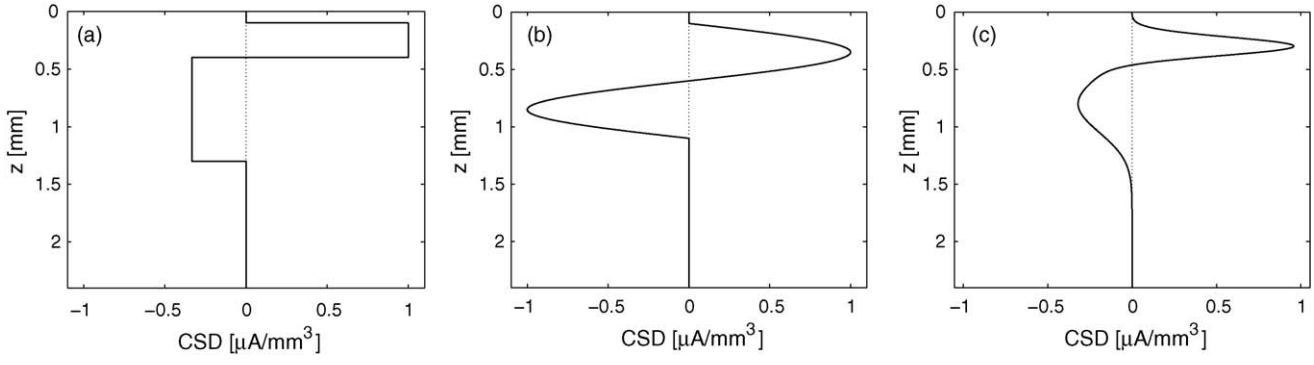

Fig. 2. Three model CSD distributions. (a) Square model function with amplitude C in the range between $z = 0.1$ and 0.4 mm and amplitude $-C/3$ between $z = 0.4$ and 1.3 mm. Zero amplitude elsewhere. (b) Sinusoidal model function given by $C \sin(2\pi(z - z_{start})/\Lambda)$ in the range $z_{start} = 0.1$ mm to $z = 1.1$ mm and zero elsewhere. Wavelength $\Lambda = 1$ mm. (c) Two-Gaussians model function, $C(\exp(-(z-\mu_1)^2/2\lambda_1^2)/\lambda_1 - \exp(-(z-\mu_2)^2/2\lambda_2^2)/\lambda_2)/\sqrt{2\pi}$ with $\mu_1 = 0.3$ mm, $\lambda_1 = 0.08$ mm, $\mu_2 = 0.8$ mm and $\lambda_2 = 0.25$ mm. The constant C is 1 μA/mm^3.

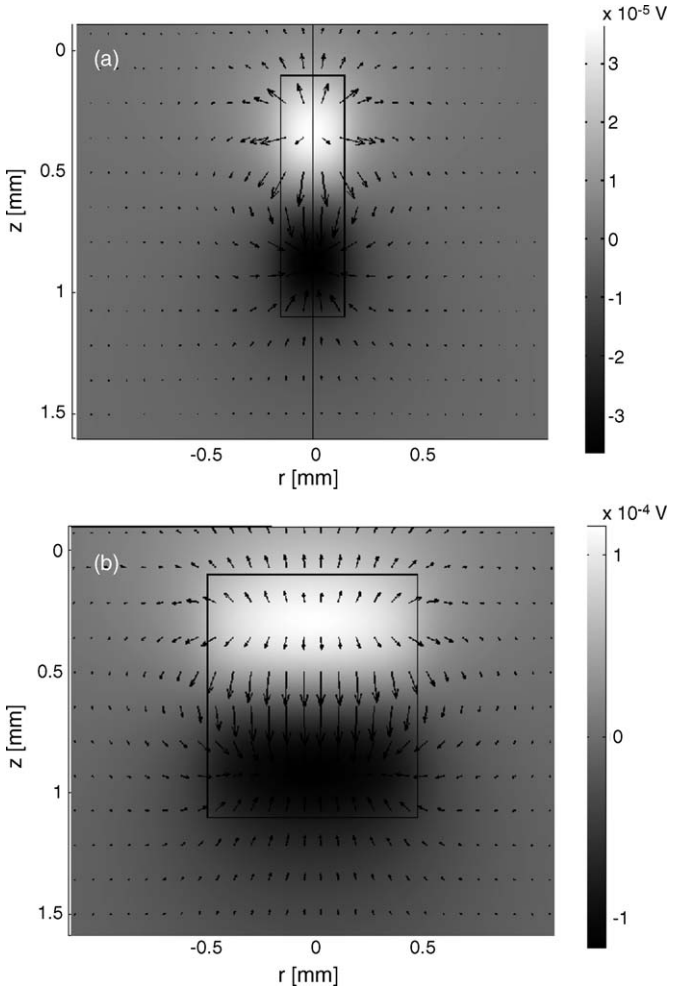

Fig. 3. Gray-scale plots of radial distribution of electrical potentials ϕ from cylindrical sources with sinusoidal model distribution in Fig. 2b with constant conductivity $\sigma = 0.3$ S/m. Arrows indicate direction and relative magnitude of current density, $\mathbf{j} = -\sigma\nabla\phi$. (a) Diameter = 0.3 mm and (b) diameter = 1.0 mm. Note that the gray-scale is different in the two plots. Plots are generated by FEMLAB (Comsol).

In Fig. 3, we show example potentials using the sinusoidal model distribution in Fig. 2 for a narrow (0.3 mm diameter) and a wide (1 mm diameter) cylindrical current-source column. For the narrow column the potential qualitatively resembles the potential around a current dipole. For the wider column the potential is seen to vary little in the lateral direction in the vicinity of the center axis. However, close to the column edge, the potential magnitudes are seen to be reduced compared to the center axis values. The plots also show the current density, $\mathbf{j} = -\sigma\nabla\phi$, illustrating how the currents flow from the sources to the sinks. According to the in-plane homogeneity assumption inherent in the standard CSD method, the currents should be directed in the vertical direction only, but due to the finite size of the cylindrical CSD this assumption is violated for finite-sized columns.

A different electrical conductivity above the cortical surface will affect the measured potential in cortex. In Fig. 4, we show the potential at the center axis for the sinusoidal model distribution for various population diameters and choices of electrical conductivity σ_0 above cortex where Eq. (13) is used to incorporate the effects of inhomogeneous conductivity. We consider the two extreme cases where $\sigma_0 \gg \sigma$, i.e., $\sigma_0 = \infty$ and $\sigma_0 \ll \sigma$, i.e., $\sigma_0 = 0$. The former mimics the situation when a highly conductive solution such as saline covers the cortical surface. The latter corresponds to coverage by an insulating liquid such as oil.

In Fig. 4, we see that for $\sigma_0 = \infty$ the potential at the cortical surface ($z = 0$) is effectively grounded to zero. For $\sigma_0 = 0$ on the other hand the spatial derivative of the potential at the cortical surface is zero. We further see that for small population diameters ($d = 0.5$ mm) the conductivity jump at the cortical surface mainly affects the potential in the top 0.5 mm of cortex. For the largest diameter ($d = 10$ mm) we see that the main effect of the conductivity jump is to give the potential an overall constant shift. This indicates that for such large diameters the CSD discs resemble infinite planes. Hence, the image sources are also infinite planes, and as long as the current sources are balanced, i.e., sum to zero, they will only give a constant shift of the potential.

3.1.2. CSD estimates for small electrode spacing

As seen in Fig. 4 the potential due to a given cylindrical current-source distribution will depend on both the cylinder diameter and the conductivity above the cortical surface. Thus, CSD estimates from the standard CSD method will in general be erroneous, regardless of how densely the potential is measured. To illustrate this we show in Fig. 5 the predicted CSD

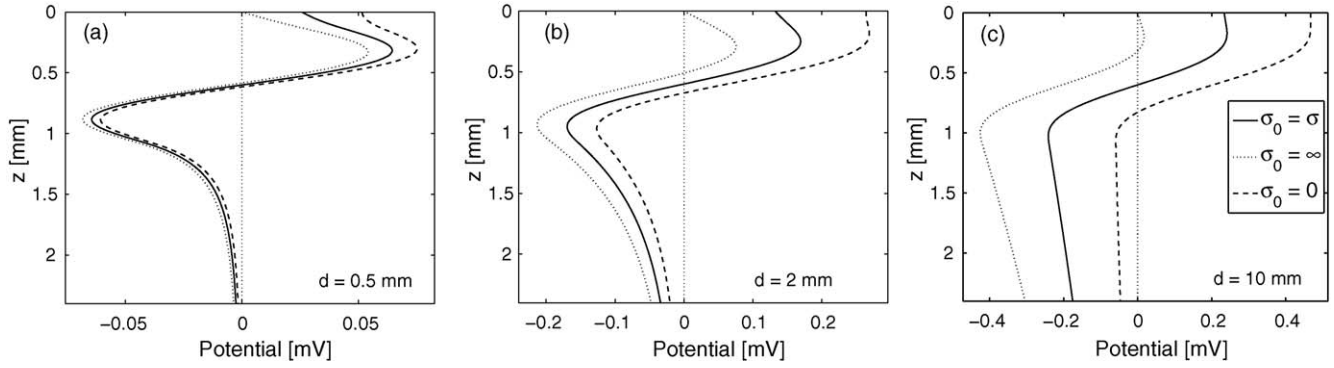

Fig. 4. Electrical potential ϕ at center axis from cylindrical sources with sinusoidal model distribution in Fig. 2b for various electrical conductivities σ_0 above cortex ($z < 0$): $\sigma_0 = \sigma$ (homogeneous, solid line), $\sigma_0 = 0$ (dashed line), $\sigma_0 = \infty$ (dotted line) and $\sigma = 0.3$ S/m. (a) Diameter=0.5 mm, (b) diameter=2 mm and (c) diameter=10 mm.

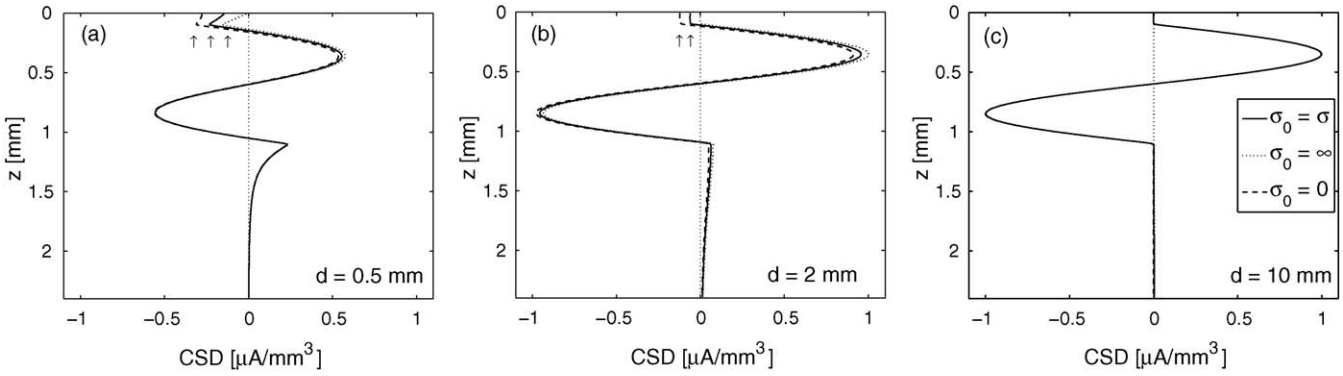

Fig. 5. Estimated CSD from standard CSD method in the limit of small electrode spacings ($h \to 0$) for sinusoidal model distribution in Fig. 2b for various electrical conductivities σ_0 above cortex ($z < 0$): $\sigma_0 = \sigma$ (homogeneous, solid line), $\sigma_0 = 0$ (dashed line) and $\sigma_0 = \infty$ (dotted line). $\sigma = 0.3$ S/m. Arrows point to spurious sinks around the top electrode. (a) Diameter = 0.5 mm, (b) diameter = 2 mm and (c) diameter = 10 mm.

profiles from the potentials in Fig. 4 when the standard CSD method in Eq. (5) is used in the limit where the electrode spacing h goes to zero. In this limit there is no error in the estimate due to finite electrode spacing.

In Fig. 5c, we see that for the largest diameter ($d = 10$ mm) the standard CSD method predicts the correct CSD distribution regardless of the conductivity jump at the cortical surface. Even though the various image sources are seen in Fig. 4c to have some effect on the shape of the potentials, they do not notably change the double spatial derivative of the potentials predicting the CSD in the standard CSD method.

In Fig. 5a, we see that for the smallest diameter ($d = 0.5$ mm) the standard CSD method predicts a spurious source immediately below the true sink. It also predicts a spurious sink immediately above the true source below the cortical surface. The size of this top spurious sink depends on the conductivity jump at the surface. The same errors are present for the intermediate diameter ($d = 2$ mm), but they are smaller.

Outside the regions around the top and bottom of the true sink–source pair, the standard CSD method is seen to predict the shape of the true CSD profile fairly well for this particular model CSD distribution. However, for the smallest diameter ($d = 0.5$ mm), the CSD amplitude is predicted to be too low by a factor of nearly two. This is due to the assumption of a CSD with infinite spatial extension while in reality the CSD is confined to a cylindrical column of limited size.

In the small h limit the inverse CSD methods will by construction predict both the correct spatial profile and amplitudes of the CSD (if the correct population diameters and conductivity distribution are assumed). For these methods the only inherent error is due to finite electrode spacing.

3.1.3. CSD estimates in limit of large cylindrical source diameters

To explore the effects of electrode spacing h on CSD estimates, we first consider the large population-diameter limit where the in-plane homogeneity approximation inherent in the standard CSD method is fulfilled. In Fig. 6, we show the predicted CSDs for the sinusoidal test distributions (with constant conductivity σ) for the various inverse CSD methods for two choices of electrode spacing h. In this large-diameter limit the δ-source iCSD method becomes equivalent to the standard CSD method for the $N - 2$ interior points. We see that the spline iCSD method is superior in predicting the correct CSD distribution. For the smaller electrode spacing ($h = 0.1$ mm) a good agreement with the true CSD is also obtained for the δ-source and step iCSD methods by interpolating between the estimated CSD point values for the δ-source iCSD method or CSD values in the middle of the step for the step iCSD method. However, for the larger electrode spacing ($h = 0.2$ mm) we see that interpolation between the estimated CSD point values for the δ-source method gives some errors, reflecting that too widely spaced δ-planes poorly approximate the true CSD distribution.

The δ-source iCSD for $h = 0.2$ mm in Fig. 6 corresponds to the spatially filtered double-derivative formula recommended by Nicholson and Freeman (1975), for grids with $h = 0.1$ mm. This estimation method has later been used by, e.g., Borroni et al. (1991), Swadlow et al. (2002). In Fig. 6 only every second estimated CSD obtained from this procedure is shown, but the results nevertheless illustrate potential additional errors inherent in this method.

3.1.4. CSD estimates for various cylindrical source diameters

We now explore how well various methods estimate the true CSD for a set of different cylindrical current-source diameters for the electrode spacing $h = 0.1$ mm. In Fig. 7, we show CSD estimates for our three model distributions given in Fig. 2 for a set of source diameters ($d = 0.1$, 0.5, 1 and 5 mm) for the δ-source and spline iCSD methods (when the conductivity σ is constant). For comparison we also show estimates from the standard CSD method augmented by the procedure of Vaknin et al. (1988) to give estimates at the first and last electrode positions.

In these model calculations the CSD estimates are based on potentials recorded at 23 electrode contacts, the first being positioned at $z = 0.1$ mm. The standard CSD method, augmented by the Vaknin procedure, and the δ-source iCSD method predicts the CSD at the 23 contact positions. The spline iCSD method predicts a continuous CSD distribution from the cortical surface ($z = 0$) to a depth of $z = 2.4$ mm.

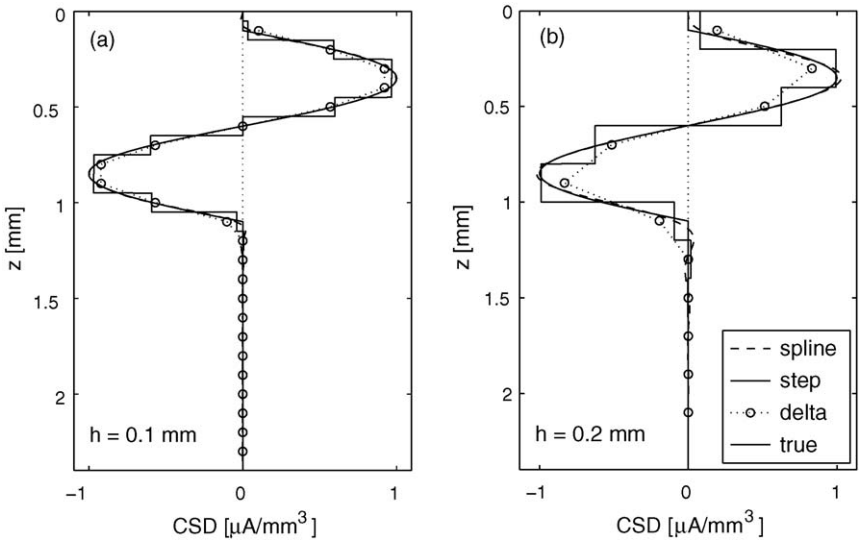

Fig. 6. Estimated CSD from inverse CSD methods for sinusoidal model distribution in Fig. 2b for large current-source diameter ($d = 10$ mm) for two choices of electrode spacings h. Constant electrical conductivity, $\sigma = 0.3$ S/m. (a) $h = 0.1$ mm, 23 electrodes with the first positioned at $z = 0.1$ mm depth. (b) $h = 0.2$ mm, 11 electrodes with the first positioned at $z = 0.1$ mm depth. Solid sinusoidal line: true CSD. Solid piecewise linear line: step iCSD. Dashed line: spline iCSD. Circles: δ-source iCSD. Dotted line linearly interpolating these points, is added to guide the eye. Note that the dashed line representing the spline iCSD estimate is mostly hidden by the solid line representing the true CSD. The δ-source results for $h = 0.2$ mm also corresponds to every second point of the spatially filtered double-derivative formula recommended by Nicholson and Freeman (1975) for grids with $h = 0.1$ mm.

A first observation is that the spline iCSD method produces excellent CSD estimates for the two 'smooth' model distributions (middle and right columns) for all population diameters. However, the square function is poorly approximated by cubic polynomials, and the predicted CSD is seen to oscillate around the true CSD in regions where the CSD changes abruptly.

The δ-source iCSD method is seen to give accurate estimates for the three largest diameters (second to fourth row). For the smallest diameter ($d = 0.1$ mm) the inherent assumption of discrete CSD distributions positioned at the electrode contact positions, is seen to lead to an underestimation of the CSD amplitudes.

The standard CSD method is seen to produce accurate CSD estimates for the 21 interior electrode positions for the largest diameter ($d = 5$ mm) where one effectively is in the in-plane homogeneous limit. For the smaller diameters the predicted CSDs for these interior positions have smaller magnitudes than the true CSD. More importantly, there are also errors in the predicted spatial profile: For the sinusoidal model distribution (middle column) a spurious source is predicted below the true sink. For the two-Gaussians distribution (right column) the sink is predicted to be too narrow and positioned too high in cortex.

The estimates at the top and bottom electrodes obtained from the procedure of Vaknin et al. (1988) assuming constant potentials immediately above and below the laminar electrode, are generally seen to have larger errors. In Fig. 7, large spurious sinks are found at the top electrode for $d = 0.1$, 0.5 and 1 mm, and notable spurious sources are seen at the bottom electrode for $d = 5$ mm. These errors are due to the inherent assumption of a constant potential around the end electrodes in their procedure. As seen in the potential plots for the sinusoidal CSD model distribution in Fig. 4 (solid lines), the potentials are generally not constant around the end electrodes even for activity diameters as large as 10 mm.

The CSD estimation error from using the standard CSD method for the $N - 2$ interior points on cylindrical current-source distributions increases with decreasing cylinder diameters. The error from applying the procedure of Vaknin et al. (1988) to obtain estimates at the top and bottom electrodes is in our model examples found to have a different diameter dependence. For our model CSDs the error at the top electrode is found to be largest for diameters of ∼1 mm or less. However, as seen in Fig. 7 it is still notable at $d = 5$ mm where the standard CSD prediction at the interior points gives excellent results. The error at the bottom electrode is found to be notable only for $d = 5$ mm.

The diameter dependence of the bottom electrode predictions following the Vaknin procedure can be qualitatively understood on physical grounds since (i) the error vanishes in the very large-diameter limit ($d \gg 5$ mm) for balanced current sources (cf. Section 2) and (ii) for very small diameters ($d \ll 5$ mm) the potentials decay rapidly with vertical distance so that the potentials around the bottom electrode from the sink–source pair in the top of cortex becomes small and slowly varying. The largest errors are thus obtained around the 'intermediate' diameter of ∼5 mm. The top electrode is located so close to the sink–source pair that significant errors are observed for all example diameters in Fig. 7.

A general conclusion is that the δ-source and spline iCSD methods overall are able to predict the CSD accurately when the positions of the electrode contact points (here equidistant at the center axis) and cylindrical source diameter are known. The same conclusion was found to apply also for the step iCSD method, but the results are not shown here. In practice the

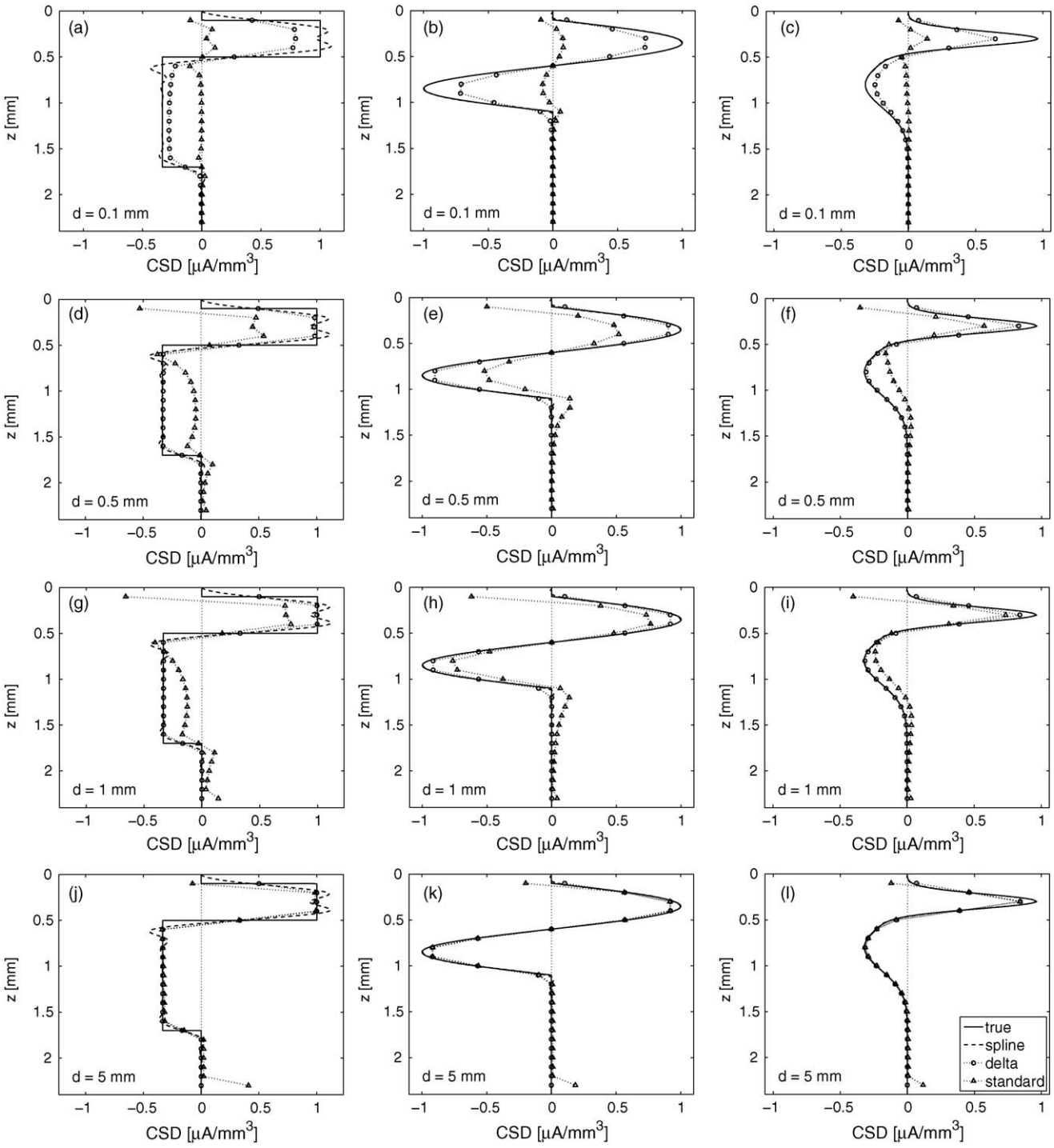

Fig. 7. Estimated CSD from inverse CSD methods and standard CSD method for the model distributions in Fig. 2 for various cylindrical source diameters d. Twenty-three electrode contacts, the first positioned at $z = 0.1$ mm. Interelectrode spacing, $h = 0.1$ mm. Constant electrical conductivity, $\sigma = 0.3$ S/m. Left column (a, d, g and j): square model function. Middle column (b, e, h and k): sinusoidal model function. Right column (c, f, i and l): two-Gaussians model function. First row (a–c): $d = 0.1$ mm. Second row (d–f): $d = 0.5$ mm. Third row (g–i): $d = 1$ mm. Fourth row (j–l): $d = 5$ mm. Solid line: true CSD. Dashed line: spline iCSD. Circles: δ-source iCSD. Triangles: standard CSD augmented by the procedure of Vaknin et al. (1988) at the the top and bottom electrodes. Dotted lines linearly interpolating these points, are added to guide the eye.

detailed laminar-electrode position and effective diameter of the cylindrical source may not be known. It is thus of interest to explore the estimation errors when incorrect assumptions are made.

In Fig. 8, we illustrate the resulting errors for the two-Gaussians model distribution when an incorrect diameter assumption is made. The true CSD diameter is 0.5 mm. When a diameter of 0.25 mm is assumed, the inverse CSD methods are seen to predict a roughly correct spatial CSD profile, but with a too high magnitude. When a too large source diameter is assumed ($d = 0.75$ mm), the CSD spatial profile is still generally

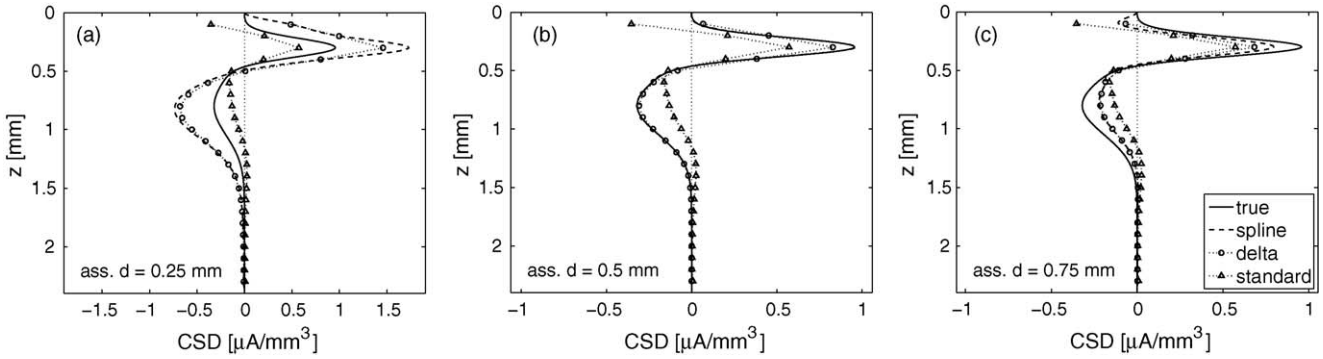

Fig. 8. Estimated CSD from inverse CSD methods and standard CSD method (augmented according to the procedure of Vaknin et al. (1988)) for the two-Gaussian model distribution in Fig. 2c assuming different cylindrical source diameters. True source diameter is $d = 0.5$ mm. (a) Assumed diameter 0.25 mm, (b) assumed diameter 0.5 mm and (c) assumed diameter 0.75 mm. Electrode contact positions, conductivity and legends as in Fig. 7.

well predicted, but now with an overall too small magnitude. We note, however, that the inverse CSD methods in this case predict a small spurious sink around the first contact, but the size is much smaller than predicted by the procedure of Vaknin et al. (1988). The standard CSD method generally performs poorer than the inverse CSD methods assuming either too small ($d = 0.25$ mm) or too large ($d = 0.75$ mm) source diameters. This is as expected since the standard CSD method inherently assumes an infinite source diameter, i.e., larger deviation from the true source diameter ($d = 0.5$ mm).

In Fig. 9, we illustrate the error due to off-center electrode position when iCSD methods assuming centered electrodes are used. In our example we consider the sinusoidal model distribution and a cylindrical source diameter of $d = 0.5$ mm. We see that when the electrode is positioned halfway between the center and the cylinder edge (b) or even at the cylinder edge (c) the 'centered' inverse CSD methods still give quite accurate predictions of the spatial profile of the CSD. However, the magnitude of the CSD is underestimated. Still, the methods perform significantly better than the standard CSD method.

3.1.5. CSD estimates assuming off-center electrode

An important advantage with the inverse CSD approach is that the method can be straightforwardly modified to incorporate known information about the system. If one, for example, after histology, finds that the laminar electrode contacts were located at the edge of cylindrical columnar activity, an appropriate iCSD estimator can be constructed as described in Section 2.5.

This is demonstrated in Fig. 10 where results from such off-center inverse CSD methods are seen to correctly predict the true CSD from potentials recorded at the appropriate off-center position. In the same figure we also show predictions from using the off-center method (constructed for electrodes positioned at the edge of cylinder source with a diameter of 0.5 mm) on potentials recorded at the cylinder center axis. Here, we see that the iCSD methods overestimate the magnitude of the CSD and predict small spurious sinks and sources above and below, respectively, the true sink–source pair. The estimation errors are also seen to be somewhat larger for the spline iCSD method.

3.1.6. CSD estimates with inhomogeneous conductivity

Another potential source for errors in the CSD estimate is inhomogeneous electrical conductivity. This is illustrated in Fig. 11 for the sinusoidal CSD distribution where the conductivity above cortex has been set to be infinitely large ($\sigma_0 = \infty$). We observe that while the spline iCSD method assuming the correct conductivity profile produces excellent CSD estimates, a spline iCSD method assuming (incorrectly) homogeneous conductivity predicts a spurious sink around the first electrode contact. We also see that these errors are comparable in size to

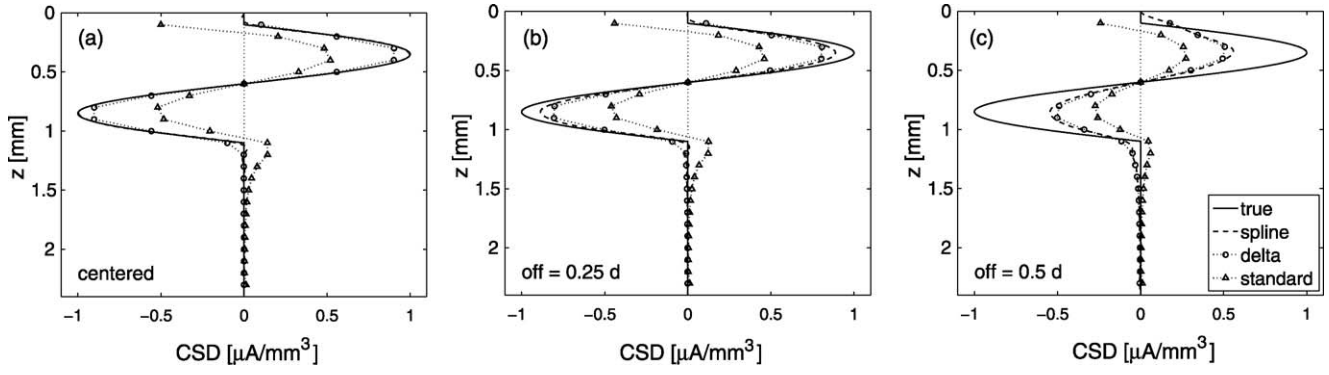

Fig. 9. Estimated CSD from inverse CSD methods and standard CSD method (augmented according to the procedure of Vaknin et al. (1988)) for the sinusoidal model distribution in Fig. 2b for different electrode positions. The iCSD methods assume centered electrodes. Cylindrical source diameter, $d = 0.5$ mm. (a) Electrode positioned in center ($r = 0$), (b) electrode positioned at $r = 0.25\,d$ and (c) electrode positioned at $r = 0.5\,d$ (at cylinder edge). Electrode intercontact distance, conductivity and legends as in Fig. 7.

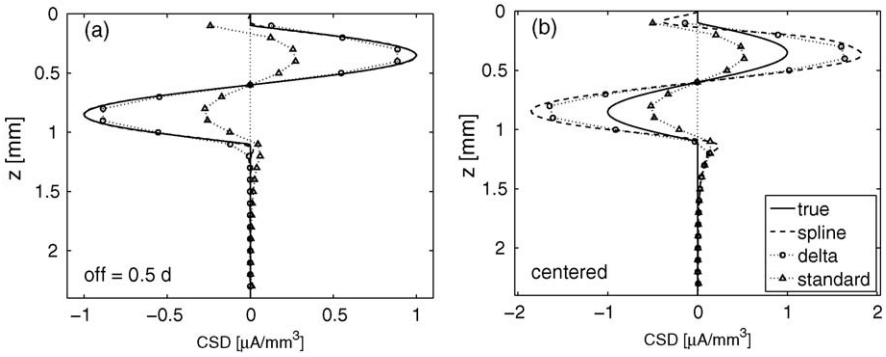

Fig. 10. Estimated CSD from off-center inverse CSD methods and standard CSD method (augmented according to the procedure of Vaknin et al. (1988)) for the sinusoidal model distribution in Fig. 2b for different electrode positions. Cylindrical source diameter, $d = 0.5$ mm. (a) Electrode positioned at cylinder edge ($r = 0.5\,d$) as assumed in the off-center inverse CSD methods. (b) Electrode positioned at center axis $r = 0$. Electrode intercontact distance, conductivity and legends as in Fig. 7.

the errors from using the procedure of Vaknin et al. (1988) at the top electrode, cf. Fig. 7.

It should thus be noted that while the effects of cylindrical confinement of current sources on the estimated CSD (assuming in-plane homogeneity as in the standard CSD method) is moderate for source diameters larger than 1 mm (cf. Fig. 7), significant errors due to conductivity jumps not appropriately accounted for, is seen around the top electrode even for diameters up to 10 mm (cf. Fig. 11).

3.1.7. CSD estimates for other current-source geometries

So far we have only considered CSD distributions with cylindrical symmetry and where the current-source discs constituting the full distributions have homogeneous current-source density in the disc plane. However, inverse CSD methods for other distribution geometries can readily be made.

Nicholson (1973) considered rectangular CSD distributions and found analytical expressions analogous to Eq. (8) for the field potential around a rectangular disc with homogeneous CSD. Thus, an inverse CSD method based on assuming this source geometry could easily be implemented.

As an alternative to homogeneous, circular current-source discs, one can, for example, assume a Gaussian planar density distribution, $C_p(r) = C_p \exp(-r^2/\Lambda_r^2)$. This models a situation where the CSD is maximum at a center axis and gradually decaying in the lateral directions. The center axis potential around this current-source disc can also be found analytically, and the resulting potential can be shown to be given by the *scaled complementary error function*.

Another variation is to consider homogeneous current-source discs with varying disc diameters. Cortical pyramidal cells often have apical dendrites with widespread branches in the topmost layers. Activation of, for example, neurons in a single column in barrel cortex may thus give a spatially wider CSD in the top layers than in the middle layers. Such a situation is demonstrated in Fig. 12 where we consider the sinusoidal model CSD distribution with a large cylindrical diameter ($d = 1$ mm) in the top ($0.1\text{ mm} < z < 0.45\text{ mm}$) and a smaller ($d = 0.5$ mm) below ($0.45\text{ mm} < z < 1.1\text{ mm}$). The total current is still balanced, i.e., the total source current equals the total sink current, but due to the varying source diameter the CSD along the center axis will not sum to zero. In the figure we see that a δ-source iCSD method assuming the correct diameter variation is able to predict the true CSD well. The corresponding δ-source iCSD method assuming a constant cylinder diameter of $d = 0.5$ mm is seen to overestimate the CSD in the upper region where the

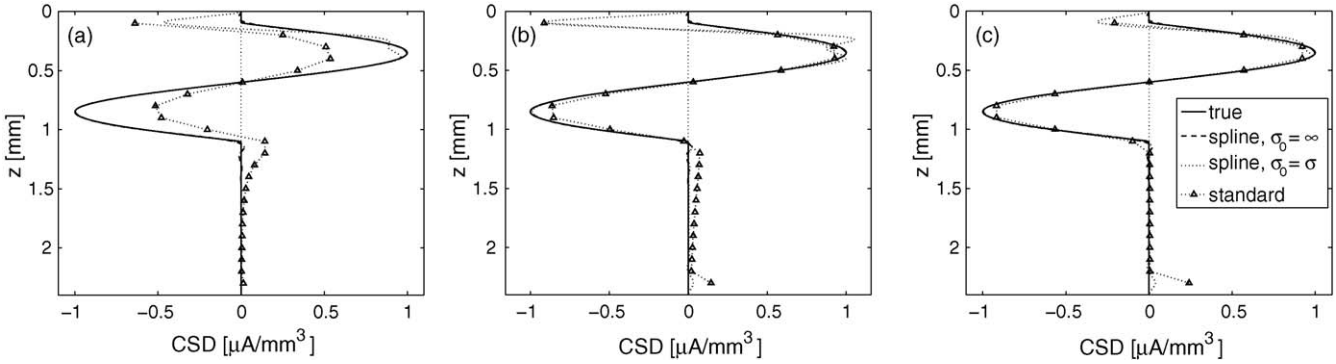

Fig. 11. Estimated CSD from inverse CSD methods and standard CSD method for the sinusoidal model distribution in Fig. 2b with infinite conductivity ($\sigma_0 = \infty$) above cortex ($z < 0$). (a) Cylindrical source diameter, $d = 0.5$ mm, (b) $d = 2$ mm and (c) $d = 10$ mm. Centered electrode positions as in Fig. 7. Solid line: true CSD. Dashed line: spline iCSD assuming $\sigma_0 = \infty$. Dotted line (without points): spline iCSD assuming homogeneous conductivity ($\sigma_0 = \sigma$). Triangles: standard CSD method using the procedure by Vaknin et al. (1988) to estimate the CSD at the first and last electrode contacts. Dotted lines linearly interpolating the respective points, are added to guide the eye.

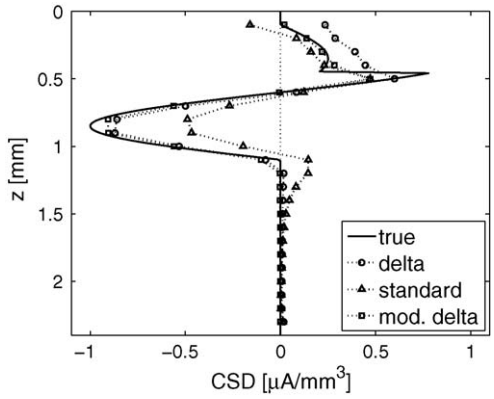

Fig. 12. Estimated CSD from various inverse CSD methods and standard CSD method for a modified sinusoidal model distribution $C(z)\sin(2\pi(z - z_{\text{start}})/\Lambda)$ in the range $z_{\text{start}} = 0.1$ mm to $z = 1.1$ mm and zero elsewhere. Wavelength $\Lambda = 1$ mm. In the range $0.1\text{ mm} < z < 0.45$ mm the current-source diameter is $d = 1$ mm and $C(z) = 0.25\ \mu\text{A/mm}^3$. In the range $0.45\text{ mm} < z < 1.1$ mm the current-source diameter is $d = 0.5$ mm and $C(z) = 1\ \mu\text{A/mm}^3$. Solid line: true CSD. Circles: δ-source iCSD assuming cylindrical source density with diameter $d = 0.5$ mm. Squares: δ-source iCSD assuming $d = 1$ mm for $0.1\text{ mm} < z < 0.45$ mm, $d = 0.5$ mm for $0.45\text{ mm} < z < 1.1$ mm. Triangles: standard CSD method using the procedure by Vaknin et al. (1988) to estimate the CSD at the first and last electrode contacts. Dotted lines linearly interpolating the respective points, are added to guide the eye. Electrode contact positions and conductivity as in Fig. 7.

true diameter is 1 mm. In the lower region where the true diameter is 0.5 mm, also this iCSD method works well. The standard CSD method gives as expected reasonable estimates in the upper large-diameter ($d = 1$ mm) region, while it provides a poor estimate in the small-diameter ($d = 0.5$ mm) region.

The sum of the estimated CSD $\hat{C}(z)$ along the center axis has been used as a measure of the accuracy of CSD estimation; a value close to zero has been taken as an indication of accurate estimates (Vaknin et al., 1988). However, for the example in Fig. 12 the CSD sum index, $\alpha_{\text{C}} = \sum_z \hat{C}(z) / \sum_z |\hat{C}(z)|$, is found to be -0.43 for the true CSD distribution and not zero. For the δ-source iCSD method assuming the correct diameter distribution, we find $\alpha_{\text{C}} = -0.46$. For the δ-source iCSD method assuming a constant disc diameter of $d = 0.5$ mm, $\alpha_{\text{C}} = -0.13$, while for the standard CSD method α_{C} is found to be exactly zero (without the top and bottom electrode estimates we get $\alpha_{\text{C}} = 0.05$).

For the standard CSD method $\sum_z \hat{C}(z)$ corresponds to the sum over discrete double spatial derivatives of the potential (cf. Eq. (4)) which adds up to the discrete single spatial derivatives at the laminar electrode end points. Thus, as long as the CSD distribution is such that the resulting potential varies little at the two topmost and lowest electrode contact points, the standard CSD method will predict a roughly balanced CSD distribution (even if this is incorrect as in the example in Fig. 12). When using the method suggested by Vaknin et al. (1988) (assuming hypothetical electrodes positioned above and below the first and last electrode with the same potential as the neighboring electrodes), these discrete spatial derivatives will be zero by construction, and α_{C} will be predicted to be exactly zero as in Fig. 12. Thus, a summation test cannot be used to justify the validity of the procedure.

3.2. Application on experimental data

Here, we apply the iCSD methods on example laminar-electrode data recordings from rat somatosensory (barrel) cortex following stimulation of the principal whisker. In Fig. 13a, the stimulus-averaged local field potentials are shown for the largest stimulus amplitude. The CSD estimate from the standard CSD method is shown in Fig. 13c. The method of Vaknin et al. (1988) is used to estimate the CSD at the first and last electrode positions, but for this example data the CSD is predicted to be close to zero at both of these positions. In Fig. 13d we show the CSD estimates resulting from spatially filtering these standard CSD-method results with a three-point low-pass Hamming filter (Ulbert et al., 2001). Note that the application of a three-point filter prevents estimates at the first and last electrodes.

In the present experiment oil was added on top of the cortical surface making it electrically insulating. In the standard CSD method the CSD estimates do not depend on such a shift in electrical conductivity, but it can be incorporated in the iCSD methods. This requires knowledge about the absolute position of the electrode contacts relative to the cortical surface. In the experiment the first contact of the laminar electrode was positioned approximatively at the cortical surface by visual control. In the example iCSD estimates shown in Fig. 13 we assume the first contact to be positioned 0.05 mm below the cortical surface.

In Fig. 13e, we show the δ-source iCSD estimate assuming the electrode contacts to be centered in a cylindrical CSD distribution with diameter $d = 0.5$ mm, and with oil ($\sigma_0 = 0$) above the cortical surface ($z < 0$). No spatial filtering has been applied to facilitate comparison with the unfiltered standard CSD estimates in Fig. 13c. We observe that the iCSD method predicts the dominant sink occurring at around 20 ms (after stimulus onset) to go deeper than the standard CSD method. Likewise, the weaker sink at later times are predicted to be larger and spatially more extended. This corresponds qualitatively to the situation seen for the two-Gaussians model distribution for $d = 0.5$ mm in Fig. 7. The δ-source iCSD method also predicts the dominant source occurring at around 20 ms to extend higher up compared to the standard CSD method, but the exact size here will depend on what position has been chosen for the first electrode contact relative to the oil interface. Note also that the iCSD method (Fig. 13e) predicts larger CSD amplitudes than the standard CSD method (Fig. 13c).

In Fig. 13f, we show the corresponding δ-source iCSD estimate when the laminar electrode is assumed to be positioned at the edge of the cylindrical CSD. The same qualitative features are predicted as in the centered iCSD estimate, but the amplitude is predicted to be about a factor two larger.

Finally, in Fig. 13b we show the CSD estimate from the spline iCSD method assuming a cylindrical CSD with $d = 0.5$ mm, centered laminar electrode, and $\sigma_0 = 0$ above the cortical surface. A Gaussian spatial filter has been applied. Note that here the CSD is predicted at each spatial point, whereas for the standard CSD and δ-source iCSD method the CSD is inherently assumed to be at the electrode contact positions. Qualitatively, the same

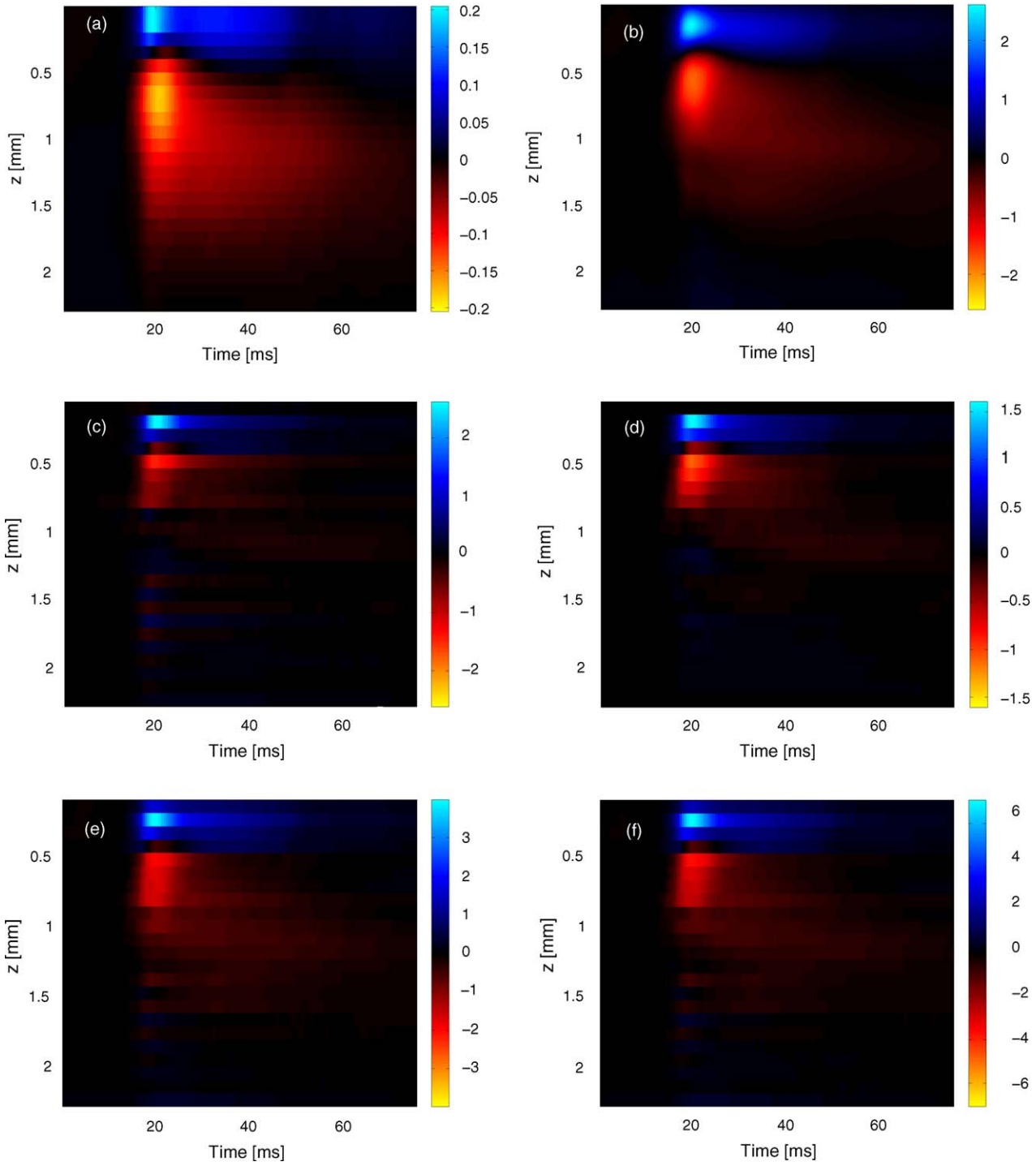

Fig. 13. Illustration of application of various CSD estimation methods on data from rat barrel cortex following stimulation of principal whisker for the largest stimulus amplitude. First electrode contact is assumed to be positioned 0.05 mm below cortical surface. (a) Stimulus-averaged local field potential. Baseline potentials have been subtracted for each electrode. $t = 0$ corresponds to stimulus onset time. (b) CSD estimate from spline iCSD method assuming oil ($\sigma_0 = 0$) at cortical surface, homogeneous CSD with diameter $d = 0.5$ mm, and laminar electrode centered at cylinder axis. CSD estimate has been spatially filtered with Gaussian filter $q(z) = \exp(-z^2/2\lambda^2)/\sqrt{2\pi}\lambda$ with $\lambda = 0.1$ mm. (c) CSD estimate from standard CSD method with method of Vaknin et al. (1988) used for estimation at first and last electrode contact. (d) Standard CSD estimate in (c) spatially filtered using a three-point Hamming filter (Ulbert et al., 2001). (e) CSD estimate from δ-source iCSD method assuming $\sigma_0 = 0$, $d = 0.5$ mm, and centered electrode. (f) CSD estimate from δ-source iCSD method assuming $\sigma_0 = 0$, $d = 0.5$ mm, and electrode positioned at edge of source cylinder ($r = 0.25$ mm). Cortical conductivity, $\sigma = 0.3$ S/m. In (a) the units on the color bar is mV. In the other panels the unit is μA/mm^3.

features are observed in the predicted CSD as for the δ-source iCSD methods.

We do not know the true spatial extension of the underlying CSD distribution or the detailed electrode position for our example data. Moreover, the sizable laminar electrode will displace the neural tissue. The correctness of the various CSD estimates in Fig. 13 is thus difficult to assess. The spatial extension of the CSD is also expected to vary with post-stimulus time, as demonstrated, for example, by surface potential recordings on the same system (Di and Barth, 1991).

The CSD stems from currents entering and leaving the extracellular volume through neuronal membranes. Since the net transmembrane current must be zero, a constraint is thus that the integrated CSD over the entire volume of current sources should sum to zero. If the sinks and sources have different lateral extensions, however, this does not imply that the summed CSD along an axis should be zero (as illustrated in Fig. 12).

As discussed above the standard CSD method will tend to give balanced estimates (i.e., sum index α_C close to zero). Further, for the example data in Fig. 13 the method of Vaknin et al. (1988) is used to get CSD estimates at the first and last electrode position, and as described in Section 3.1.7 the CSD summing index α_C will be identically zero for the unfiltered case (Fig. 13c). For the filtered standard CSD estimates α_C is found to be around -0.1. The various inverse CSD estimates assuming $d = 0.5$ mm are found to have α_C in the range -0.1 to -0.25. As illustrated by Fig. 12 negative values of α_C could reflect that the sinks have narrower spatial extensions than the sources.

4. Discussion

In the present paper we have introduced a new method for estimation of current-source density based on inversion of the electrostatic forward solution. The method, labeled the inverse CSD method, can be applied to data from various types of multielectrode geometries. Here, we have focused on linear-array (laminar) electrodes which is commonly used to probe cortical population activity. The standard method for CSD estimation from such potential recordings has been to apply a three-point discrete spatial double derivative filter, often in combination with a three-point discrete spatial low-pass filter. This procedure is based on the assumption of a CSD homogeneously distributed in infinite planes aligned with the cortical layers.

A set of different iCSD methods have been considered. In the methodologically simplest, the δ-source iCSD method, the current sources are assumed to be homogeneously distributed in infinitely thin, circular discs. When the discs are positioned at the electrode contacts, the method is, in the limit of infinite disc diameters, found to correspond to the standard CSD method. Further, the method of Vaknin et al. (1988) for supplementing the standard CSD method with estimates at the first and last electrodes, are found to be correct in the infinite source diameter limit as long as the CSD is balanced (total sink current equals total source current).

Two other iCSD methods have also been considered: the step iCSD method, assuming a step-wise constant CSD between the electrode contacts, and the spline iCSD method where a smooth CSD is constructed by interpolation of a set of cubic polynomials. Tests with model distributions show, as expected, that the spline iCSD methods are superior in correctly predicting the detailed shape of smooth CSD distributions. However, also the δ-source and step iCSD methods are found to generally give good estimates.

For cylindrical model CSD distributions with diameters less than $\sim$1 mm, the standard CSD method (inherently assuming an infinite source diameter) is seen to give erroneous CSD estimates, e.g., spurious sinks and/or sources. The iCSD estimates are seen to be more accurate, even when somewhat incorrect assumptions regarding spatial extension of current sources or electrode positions are made.

While the iCSD methods naturally produce CSD estimates around all N electrode contacts, the standard CSD method only produces estimates at the $N - 2$ interior contact positions. To produce CSD estimates at top and bottom electrode positions, the standard CSD method is commonly augmented using the procedure of Vaknin et al. (1988). While this procedure are shown to in principle be correct in the infinite-diameter limit with balanced current sources, sizable errors were observed even for CSD diameters of several millimeters.

Discontinuities in the extracellular conductivity at, for example, the cortical surface may also produce errors in the CSD estimates for electrode positions close to the conductivity jump. While this error also vanishes in the infinite-diameter limit with balanced sources, sizable errors were observed even for diameters of several millimeters. With the correct spatial distribution of conductivity implemented using the method of images, the iCSD methods avoid this error.

Effects on the CSD estimates from assuming spatially confined sources were demonstrated on experimental laminar-electrode data from the rat somatosensory (barrel) cortex. Since we do not a priori know the lateral spatial extension of the CSD, it is difficult to assess what the most correct CSD estimate is for this particular example. The advantage of the iCSD approach, however, is that if additional information about, say, detailed electrode position is available, it can be utilized in the estimation procedure. Further, the method can directly be extended to benefit from more comprehensive recordings using, for example, multishank electrodes (Buzsaki, 2004) or combinations of surface and laminar electrodes (Menzel and Barth, 2005). With potentials recorded in more than one spatial dimension, the iCSD methods can potentially give reliable estimates of both the lateral and vertical CSD distributions.

However, even when only data from a single laminar electrode is available, the present methods can aid in the data interpretation by checking the validity of the CSD estimates. By performing a set of estimates for the full range of probable or possible system parameters (for example, source diameter), robust features of the CSD predictions can be identified. Observed features in the predicted CSD which are found to depend sensitively on a particular choice of value for an (uncertain) system parameter, should be mistrusted.

Since the iCSD methods are based on Eq. (1) and thus the quasistatic approximation (Nicholson and Freeman, 1975), time and

space are essentially decoupled as in the standard CSD method. However, one can imagine an iCSD analysis assuming a time-dependent CSD diameter to mimic varying spatial extensions of neural activity after stimulation onset (Di and Barth, 1991).

The standard CSD method requires the distance between the electrode contacts to be constant. The iCSD method can straightforwardly be generalized to the case where the distance between electrode contact points vary. This could be an advantage if, say, a particular electrode contact in a laminar electrode is dysfunctional so that accurate potentials measurements are unavailable. Then this particular electrode can simply be omitted from the CSD analysis. In the present iCSD methods the only constraint is that the number N_e of electrodes recording potentials and the number N_p of parameters determining the CSD distribution are equal. In the applications presented here the vertical spatial regions of CSD described by each estimated CSD value, were assumed to be the same (the interelectrode distance h for the step and spline iCSD methods). However, one could alternatively, say, use more parameters to describe the CSD distributions in the cortical layers where the CSD is large and rapidly changing with spatial positions, if less parameters are used to describe other regions. Alternatively, one can describe the CSD distribution with less than N_e parameters to make the system overdetermined. Standard linear optimization techniques can then be used to determine the best fit, i.e., the best CSD estimate (Gershenfeld, 1999).

It is difficult to give a general recommendation on which of the iCSD methods to use. The δ-source method is generally easier to implement and requires the least numerical computation, but can give inaccurate estimates if the electrode spacing is too large. Both the δ-source and step iCSD methods can straightforwardly be modified to complex source geometries (such as varying disc diameter, cf. Fig. 12) whereas the spline iCSD method is more difficult to implement is such situations. Given the expected smooth changes in the CSD, the spline iCSD method appears to be the natural choice, but the method can be more sensitive to spatial noise. Again a natural strategy is to use several methods on the same field potential data to identify robust features in the predictions.

The focus in this article has been on interpretation of local field potentials, i.e., the low-frequency part of extracellularly recorded potentials. A similar approach using the forward solution has recently been pursued to interpret extracellular signatures of action potentials (Somogyvari et al., 2005).

Acknowledgements

We thank Martin Kermit for help with the data processing. This work was supported by the National Institute of Health Grants R01 EB00790 and NS18741 and by the Research Council of Norway.

Appendix A. δ-Source iCSD estimator for large and small R

A.1. Large R

When R becomes much larger than the spatial extension of the laminar electrode (Nh), we find

$$\mathbf{F}^{-1} = -\frac{\sigma}{h^2}\begin{bmatrix} -(1+h/R) & 1 & 0 & 0 & 0 \dots & \dots & 0 \\ 1 & -2 & 1 & 0 & 0 \dots & \dots & 0 \\ 0 & 1 & -2 & 1 & 0 \dots & \dots & 0 \\ . & . & . & . & \dots & \dots & . \\ 0 & 0 & \dots & & \dots 0 & 1 & -2 \quad 1 \\ 0 & 0 & \dots & & \dots 0 & 0 & 1 \quad -(1+h/R) \end{bmatrix}. \tag{16}$$

Comparison of this $N \times N$ matrix with the $(N-2) \times N$ matrix $-\sigma\mathbf{D}_1$ in Eq. (6), shows that $-\sigma\mathbf{D}_1$ is identical to the $N-2$ internal rows of $\mathbf{F}^{-1}$. Thus the inverse CSD method assuming infinitely thin current-source planes at the electrode positions is equivalent to the standard CSD method for the $N-2$ interior electrode contacts.

The inverse δ-source iCSD method also immediately predicts the CSD at the first and last electrode positions, whereas these are not immediately predicted by the standard CSD method. Vaknin et al. (1988) suggested a procedure for supplementing the standard method with CSD estimates at the first and last electrode positions. For example, for the first electrode position they assumed a hypothetical electrode (labeled 0) positioned a distance h above the first electrode measuring the same potential as the first electrode, i.e., $\phi_0 = \phi_1$. With the additional hypothetical electrode, the predicted CSD at the first electrode will according to the standard CSD method in Eq. (5) be $\hat{C}_1 = -\sigma(\phi_0 - 2\phi_1 + \phi_2)/h^2 = -\sigma(-\phi_1 + \phi_2)/h^2$. This corresponds to the results from the δ-source iCSD method, cf. first row of Eq. (16), *when the term of order h/R is omitted*. As shown below the terms of order h/R can be omitted in the large R limit *when the planar current sources densities are balanced*, i.e., $\sum_i C_i = 0$. Thus in this situation the standard CSD method, supplemented with Vaknin-estimates at the first and last electrode positions, gives estimates in complete accordance with the δ-source iCSD method. However, when the current sources densities are unbalanced, i.e., $\sum_i C_i \neq 0$, the h/R terms must be retained, and the Vaknin procedure generally gives incorrect estimates at the first and last electrode positions.

In the large R limit we find from Eq. (9) that the field potential ϕ_j at position z_j is given by

$$\phi_j = \sum_{i=1}^{N} \frac{h^2}{2\sigma}\left(\sqrt{(j-i)^2+(R/h)^2} - |j-i|\right) C_i$$
$$\simeq \sum_{i=1}^{N} \frac{h^2}{2\sigma}(R/h - |j-i|)C_i. \quad (17)$$

The estimated CSD at the first electrode position, $\hat{C}_1$ is then found from Eq. (16) to be

$$\hat{C}_1 = \frac{\sigma}{h^2}(\phi_1(1+h/R) - \phi_2)$$
$$= \sum_{i=1}^{N} \frac{1}{2}\left(-|i-1| + |i-2| + \frac{R}{h}\frac{h}{R} - \frac{|i-1|h}{R}\right) C_i$$
$$\simeq \sum_{i=1}^{N} \frac{1}{2}\left(-|i-1| + |i-2| + 1\right) C_i, \quad (18)$$

where we have omitted the term of order h/R in the final step. Inspection of the sum in Eq. (18) shows that the terms with $i \geq 2$ are zero. The only contribution comes from $i = 1$, and we find $\hat{C}_1 = C_1$ as we should. This argument can also straightforwardly be modified to show that the CSD estimator in Eq. (16) for the last electrode ($\hat{C}_N$) gives the correct result.

Note that without the term $(-h/R)$ in $\mathbf{F}_{11}^{-1}$, we would get the estimator

$$\hat{C}_1 \simeq \sum_{i=1}^{N} \frac{1}{2}\left(-|i-1| + |i-2|\right) C_i = C_1 - \frac{1}{2}\sum_{i=1}^{N} C_i. \quad (19)$$

Thus as long as the current-source densities are balanced, i.e., $\sum_i C_i = 0$, the term $(-h/R)$ can be omitted from $\mathbf{F}_{11}^{-1}$ (and likewise from $\mathbf{F}_{NN}^{-1}$).

A.2. Small R

It is also of interest to study the limit where R/h becomes small, i.e., the sources become much smaller than the electrode spacing. From Eq. (10) we find that in this limit

$$F_{jj} = \frac{h^2}{2\sigma}\frac{R}{h}, \qquad F_{ji} \simeq \frac{h^2}{2\sigma}\frac{1}{2|j-i|}\left(\frac{R}{h}\right)^2, \; j \neq i. \quad (20)$$

Thus $F_{ji}/F_{jj} \propto R/h$ which approaches zero in this small-source limit. Thus, the matrix $\mathbf{F}$ as well as $\mathbf{F}^{-1}$ will become diagonal, which demonstrates that for very small sources the best estimate of the CSD will simply be proportional to the potential itself (and not the double spatial derivative of the potential).

Appendix B. Spline iCSD method

In the spline iCSD method the variation of the CSD in the z-direction is modeled as a set of cubic polynomials $p_i(z)$,

$$p_i(z) = a_{i0} + a_{i1}(z-z_i) + a_{i2}(z-z_i)^2 + a_{i3}(z-z_i)^3,$$
$$z_i \leq z \leq z_{i+1}. \quad (21)$$

The polynomial $p_i(z)$ describes the vertical CSD distribution between electrode contact positions i and $i+1$. In addition to the N electrode contact positions we also incorporate two 'virtual' electrode contacts $i = 0$ and $i = N+1$ and consider the whole spatial interval between these two virtual contacts (positioned at z_0 and z_{N+1}, respectively). Thus, the CSD is constructed by incorporating polynomials $p_i(z)$ from Eq. (21) with $i = 0, \ldots, N$.

In the following we assume that the CSD at these virtual contact points above and below the electrode contact points are zero, i.e., $C(z_0) = C(z_{N+1}) = 0$. We further assume that the spatial derivative k (in the z-direction) of the CSD is zero at these positions, i.e., $k_0 = C'(z_0) = 0$ and $k_{N+1} = C'(z_{N+1}) = 0$. This assumes that the top virtual electrode is positioned at or above the cortical surface and the low virtual electrode is at or below the bottom boundary of the cortical layers.

Given that one knows the values of the CSD at the N real and two virtual electrode contact positions, $C(z_i) = C_i$, the first requirement when constructing the CSD function with cubic splines is that

$$p_i(z_i) = C_i, \qquad p_i(z_{i+1}) = C_{i+1}, \quad i = 0, \ldots, N. \quad (22)$$

When one further requires the first and second derivatives at the interface points z_i, $i = 1, \ldots, N$, to be continuous (and assumes $k_0 = k_{N+1} = 0$) it follows that there exists one and only one cubic spline fulfilling all the above criteria (Kreyzig, 1999). Thus, the coefficients a_{i0}, a_{i1}, a_{i2} and a_{i3} for $i = 0, \ldots, N$ will be uniquely determined by the values of C_i and k_i for $i = 0, \ldots, N+1$.

The contribution to the potential at position z_j from the current sources assigned to the cubic polynomial $p_i(z)$ is given by

$$\phi(z_j) = \frac{1}{2\sigma}\int_{z_i}^{z_i+h} \sum_{m=0}^{3} a_{im}(z'-z_i)^m$$
$$\times \left(\sqrt{(z_j-z')^2+R^2} - |z_j-z'|\right) \mathrm{d}z'. \quad (23)$$

The integral for $m = 0$ corresponds to the integral for the step-wise constant iCSD method which can be solved analytically. Also the other integrals (for $m = 1, 2$ and 3) can be solved analytically, but we do not list the resulting formulas here.

From the theory of cubic splines (Kreyzig, 1999) one has the following relationship between the CSDs ($C(z_i) = C_i$) and spatial derivatives ($k_i = C'(z_i)$)

$$c_{i-1}k_{i-1} + 2(c_{i-1}+c_i)k_i + c_i k_{i+1}$$
$$= 3(c_{i-1}^2(C_i - C_{i-1}) + c_i^2(C_{i+1} - C_i)) \quad (24)$$

where $c_i = 1/(z_{i+1} - z_i)$, $i = 1, \ldots, N$. Further, the coefficients of the polynomials of Eq. (21) are given by (Kreyzig, 1999) $a_{i0} = C_i$, $a_{i1} = k_i$, $a_{i2} = 3c_i^2(C_{i+1} - C_i) - c_i(k_{i+1} + 2k_i)$ and $a_{i3} = 2c_i^3(C_i - C_{i+1}) + c_i^2(k_{i+1} + k_i)$.

The equation system represented by Eq. (24) may be expressed in matrix form as $\mathbf{K} = \mathbf{TC}$ where $\mathbf{K}$ and $\mathbf{C}$ are column vectors of length $N+2$, i.e., $\mathbf{K} = [k_0\ k_1\ \ldots\ k_{N+1}]^{\mathrm{T}}$ and $\mathbf{C} = [C_0\ C_1 \ldots C_{N+1}]^{\mathrm{T}}$, and $\mathbf{T}$ has dimension $(N+2) \times (N+2)$. The set of coefficients may also be expressed in matrix

form, $\mathbf{A}_0 = \mathbf{E}_0\mathbf{C}, \mathbf{A}_1 = \mathbf{E}_0\mathbf{K} = \mathbf{E}_0\mathbf{T}\mathbf{C} = \mathbf{E}_1\mathbf{C}$, $\mathbf{A}_2 = \mathbf{B}_2\mathbf{C} + \mathbf{D}_2\mathbf{K} = \mathbf{E}_2\mathbf{C}, \mathbf{A}_3 = \mathbf{B}_3\mathbf{C} + \mathbf{D}_3\mathbf{K} = \mathbf{E}_3\mathbf{C}$. Here, $\mathbf{A}_m$ is the $N+1$-dimensional column vector $\mathbf{A}_m = [a_{0m}\, a_{1m}\, \ldots\, a_{Nm}]^{\mathrm{T}}$, and the matrices $\mathbf{E}_0, \ldots, \mathbf{E}_3$ have dimensions $(N+1) \times (N+2)$. In the operation $\mathbf{E_0C}$ (and $\mathbf{E_0K}$), the matrix $\mathbf{E}_0$ removes the last element of the vector $\mathbf{C}$ (or $\mathbf{K}$). The matrices $\mathbf{B}_2, \mathbf{D}_2, \mathbf{B}_3$, and $\mathbf{D}_3$ are constructed directly from the coefficients a_{i0}, a_{i1}, a_{i2} and a_{i3} above. $\mathbf{T}$ is constructed from Eq. (24).

The potential at the N electrode contact points can now be expressed in matrix form as

$$\mathbf{\Phi} = \mathbf{F}_0\mathbf{A}_0 + \mathbf{F}_1\mathbf{A}_1 + \mathbf{F}_2\mathbf{A}_2 + \mathbf{F}_3\mathbf{A}_3, \tag{25}$$

with $\mathbf{F}_m$ $(m = 0, \ldots, 3)$ having dimension $N \times (N+1)$ and matrix elements

$$F_{ji}^m = \frac{1}{2\sigma}\int_{z_i}^{z_i+h} (z' - z_i)^m \times \left(\sqrt{(z_j - z')^2 + R^2} - |z_j - z'|\right) \mathrm{d}z', \tag{26}$$

where $j = 1, 2, 3, \ldots, N$ and $i = 0, 1, 2, \ldots, N$. These integrals can be evaluated exactly.

Since all the $\mathbf{A}$-matrices can be expressed by $\mathbf{C}$ as shown above, we then find from Eq. (25)

$$\mathbf{\Phi} = (\mathbf{F}_0\mathbf{E}_0 + \mathbf{F}_1\mathbf{E}_1 + \mathbf{F}_2\mathbf{E}_2 + \mathbf{F}_3\mathbf{E}_3)\,\mathbf{C} = \mathbf{F}\mathbf{C}, \tag{27}$$

where the matrix $\mathbf{F}$ has dimension $N \times (N+2)$.

The matrix $\mathbf{F}$ relates the N values of the potential ($\mathbf{\Phi}$) with $N+2$ values of the CSD ($\mathbf{C}$). To make the estimation well-posed two more conditions are needed, and this is provided by the assumption that $C(z_0) = C(z_{N+1}) = 0$, i.e., no CSD on the two virtual contact points at the ends. These conditions are incorporated mathematically by inserting two extra elements to the matrix containing the potentials, so that $\mathbf{\Phi} = [\phi_1\, \phi_2\, \ldots\, \phi_N]^{\mathrm{T}} \rightarrow \mathbf{\Phi}_{N+2} = [0\, \phi_1\, \phi_2\, \ldots\, \phi_N\, 0]^{\mathrm{T}}$. In addition, the matrix $\mathbf{F}$ must be made into a $(N+2) \times (N+2)$ matrix ($\mathbf{F} \rightarrow \mathbf{F}_{N+2}$) by inserting an extra top row containing $[1\,0\,0\ldots\,0]$ and an extra bottom row $[0\,0\,0\ldots\,1]$. $\mathbf{F}_{N+2}$ is now a square invertible matrix, so that an estimator $\hat{\mathbf{C}}$ is given by

$$\hat{\mathbf{C}} = \mathbf{F}_{N+2}^{-1}\mathbf{\Phi}_{N+2}. \tag{28}$$

From the N experimentally measured values of the potential ϕ, we can now estimate the values of the CSD at the electrode contact positions. We can then use the coefficients $\mathbf{A}_m$ listed above to determine the polynomials in Eq. (21), and thus the CSD between z_0 and z_{N+1}, completely.

References

Borroni AM, Vaknin G, Berry R, Teyler T. Methods for studying the conductance changes associated with synaptic activation of forebrain slices: the interpretation of field potentials using CSD profiles. J Neurosci Methods 1991;39:89–102.

Buzsaki G. Large-scale recording of neuronal ensembles. Nat Neurosci 2004;7:446–51.

Dale AM. Optimal experimental design for event-related fMRI. Hum Brain Map 1999;8:109–14.

Devor A, Dunn AK, Andermann ML, Ulbert I, Boas DA, Dale AM. Coupling of total hemoglobin concentration, oxygenations, and neural activity in rat somatosensory cortex. Neuron 2003;39:353–9.

Devor A, Ulbert I, Dunn AK, Narayanan SN, Jones SR, Andermann ML, Boas DA, Dale AM. Coupling of the cortical hemodynamic response to cortical and thalamic neural activity. Proc Nat Acad Sci USA 2005;102:3822–7.

Di S, Barth DS. Topographic analysis of field potentials in rat vibrissa/barrel cortex. Brain Res 1991;546:106–12.

Freeman JA, Nicholson C. Experimental optimization of current-source density technique for anuran cerebellum. J Neurophysiol 1975;38:369–82.

Gershenfeld, N. The nature of mathematical modelling. Cambridge: New York, 1999.

Hämäläinen M, Hari R, Ilmoniemi RJ, Knuutila J, Lounasmaa OV. Magnetoencephalography theory, instrumentation, and applications to noninvasive studies of the working human brain. Rev Mod Phys 1993;413–97.

Hubel D, Wiesel TN. The functional architecture of the macaque visual cortex. Proc Roy Soc B 1977;198:1–59.

Jackson JD. Classical Electrodynamics. 3rd edition. New York: Wiley; 1998.

Kreyzig E. Advanced Engineering Mathematics. 8th edition. New York: Wiley; 1999.

Menzel RR, Barth DS. Multisensory and secondary sensory somatosensory cortex in the rat. Cerebral Cortex 2005;15:1690–6.

Mitzdorf U. Current source-density method and application in cat cerebral cortex: Investigation of evoked potentials and EEG phenomena. Physiol Rev 1985;65:37–100.

Mountcastle VB. The columnar organization of the neocortex. Brain 1997;120:701–22.

Nadasdy Z, Csicsvari J, Penttonen M, Hetke J, Wise K, Buzsaki G. Extracellular recording and analysis of neuronal activity: From single cells to ensembles. In: Eichenbaum H, Davis JL, editors. Neuronal Ensembles. New York: Wiley; 1998. p. 17–56.

Nakagawa H, Matsumoto N. Current source density analysis of ON/OFF channels in the frog optic tectum. Prog Neurobiol 2000;61:1–44.

Nicholson C, Llinas R. Field potentials in the alligator cerebellum and theory of their relationship to Purkinje cell dendritic spikes. J Neurophysiol 1971;34:509–31.

Nicholson C. Theoretical analysis of field potentials in anisotropic ensembles of neuronal elements. EEE Trans Biomed Eng 1973;20:278–88.

Nicholson C, Freeman JA. Theory of current source-density analysis and determination of conductivity tensor for anuran cerebellum. J Neurophysiol 1975;38:356–68.

Nicholson C, Llinas R. Real time current source-density analysis using multielectrode array in cat cerebellum. Brain Res 1975;100:418–24.

Pettersen KH, Cavero M, Einevoll GT. Cylindrical current source density: An alternative model for computing the current source density. Soc Neurosci Abs 2004;921.14.

Rappelsberger P, Pockberger H, Petsche H. Current source density analysis: methods and application to simultaneously recorded field potentials of the rabbit's visual cortex. Pflügers Arch 1981;389:159–70.

Somogyvari Z, Zalanyi L, Ulbert I, Erdi P. Model-based source localization of extracellular action potentials. J Neurosci Methods 2005;147:126–37.

Swadlow HA, Gusev AG, Bezdudnaya T. Activation of a cortical column by a thalamocortical impulse. J Neurosci 2002;22:7766–73.

Ulbert I, Halgren E, Heit G, Karmos G. Multiple microelectrode-recording system for human intracortical applications. J Neurosci Methods 2001;106:69–79.

Vaknin G, DiScenna PG, Teyler TJ. A method for calculating current source density (CSD) analysis without resorting to recording sites outside the sampling volume. J Neurosci Methods 1988;24:131–5.

Woolsey TA, Van der Loos H. The structural organization of layer IV in the somatosensory region (SI) of mouse cerebral cortex. Brain Res 1970;17:205–42.